

**FINITE ELEMENT ANALYSIS OF EXTERNALLY
PRESTRESSED SEGMENTAL
CONSTRUCTION**

by

KAMAL CHAKIB EL-HABR, B.S.

THESIS

Presented to the Faculty of the Graduate School of

The University of Texas at Austin

in Partial Fulfillment

of the Requirements

for the Degree of

MASTER OF SCIENCE IN ENGINEERING

THE UNIVERSITY OF TEXAS AT AUSTIN

May 1988

Copyright

by

Kamal Chakib El-Habr

1988

TABLE OF CONTENTS

Chapter	Page
1. INTRODUCTION	1
2. FINITE ELEMENT FORMULATION	3
2.1 Beam Element	3
2.2 External Tendon Element	12
2.3 Joint Element	16
3. SOLUTION PROCEDURE	22
3.1 Linearization	24
3.2 Equation Solution	24
3.3 State Determination	24
4. VERIFICATION OF FORMULATION	27
5. APPLICATION	37
6. SUMMARY AND CONCLUSIONS	65
APPENDIX A USER INSTRUCTIONS FOR COMPUTER PROGRAM	66
APPENDIX B GEOMETRY AND STRESSES FOR EXTERNAL TENDONS IN CHAPTER 5	84
REFERENCES	88
VITA	89

LIST OF TABLES

Table	Page
4.1 Results of Example 4.1	28
4.2 Results of Example 4.2	30
4.3 Midspan Load-Displacement and Joint Opening Fraction for Examples 4.4 to 4.7	35
5.1 Model for Regular and Pier Segments	45
5.2 Material Properties for Concrete Segments and Reinforcing Steel . .	47
A.1 Title and Control Information Formats	67
A.2 Data Input: Macro Control Statements	69
A.3 Coordinate Data	70
A.4 Element Data	71
A.5 Material Property Data	72
A.6 Boundary Restraint/Joint Specification Data	75
A.7 Nodal Force Boundary Value Data	76
A.8 Input Data for Externally Prestressed Segmental Bridge of Fig. A.1	77
A.9 List of Macro Programming Commands	80
A.10 Proportional Load Data	82

LIST OF FIGURES

Figure	Page	
2.1	Finite element model for a simple span, segmental bridge with external tendons	4
2.2	Beam element model	4
2.3	Stress-strain relationships for (a) concrete and (b) reinforcing steel .	7
2.4	Reinforced-concrete fiber cross section	9
2.5	External tendon element model	14
2.6	Compatibility relationships of the tendon element	14
2.7a	Gap between segments	18
2.7b	Force-displacement relationship of the joint	18
2.8	Joint element model	18
2.9	Four states of the joint element	20
3.1	Iteration methods: (a) Newton-Raphson iteration and (b) modified Newton-Raphson iteration (K_{ij} is reformed every two iterations.)	23
3.2	Effect of path dependence: (a) monotonous loading (b) unloading .	25
4.1	Finite element layout for Example 4.1	28
4.2	Finite element layout for Example 4.2	30
4.3	Finite element model for verification of Example 4.3	31
4.4	Midspan load-displacement curves for Bresler-Scordelis (as in Ref. 3) experiment and finite element analysis of Example 4.3 .	32
4.5	Finite element model for Examples 4.4 to 4.7	33
4.6	Midspan load-displacement curves for Examples 4.4 to 4.7	36
5.1	Three span segmental bridge	38
5.2a	Regular segment cross section	39
5.2b	Pier segment cross section	40
5.3	External tendon profile for segmental bridge (geometry and stress are given in Fig. B.1)	41
5.4a	Regular segment fiber model	43

5.4b	Pier segment fiber model	43
5.5	Stress-strain relationship for concrete segments	46
5.6	Stress-strain relationship for reinforcing steel	46
5.7	Stress-strain relationship for external tendons	48
5.8	Live load-displacement curves at interior midspan	48
5.9	Live load versus percentage opening of joint at interior midspan . .	49
5.10	Live load versus interior midspan stress of tendon B	49
5.11	Live load-displacement curves at interior midspan	52
5.12	Live load versus joint percentage opening at interior midspan . . .	53
5.13	Live load versus interior midspan stress of tendon B	54
5.14	Service live loads	55
5.15	Joint percentage openings and widths for load factors 4.0 and 6.5 of LS1 for all joints	56
5.16	Load factor for LS1 versus percentage opening of specified joints . .	58
5.17	Load factor of LS1 versus stresses of specified tendons at critical joints	60
5.18	Load factor of LS1 versus top and bottom concrete fiber stresses at specified locations (See Fig. 5.15.)	60
5.19	Joint percentage openings and widths for load factors 4.5 and 6.0 of LS2 for all joints	61
5.20	Load factor of LS2 versus percentage openings of specified joints . .	63
5.21	Load factor of LS2 versus stresses of specified tendons at critical joints	63
5.22	Load factor of LS2 versus top and bottom concrete fiber stresses at specified locations (See Fig. 5.19.)	64
A.1	Mesh for externally prestressed segmental bridge with two segments	83
B.1	Geometry and prestressing forces at transfer and after losses for each tendon	85

1. INTRODUCTION

Since the first completions of segmental bridges in the 1950's and 1960's in Europe, and in the 1970's in the United States, design and construction of segmental prestressed concrete box girder bridges has become a predominant form of medium and long-span bridge construction (100 to 650 feet span), and has been characterized by rapid evolution. Economic factors have continually suggested refinements in construction practices to increase productivity and minimize construction time. Each of these developments in construction methods has required innovative design procedures. Principal among these are the relocation of tendon anchorage zones, the use of multiple shear keys, the omission of epoxy from the joints, and the use of tendons external to the webs and flanges.

Relatively little analytical investigation has been undertaken to predict the behavior of segmental bridges under the new developments for all ranges of loads. A significant number of segmental prestressed concrete box girder bridges with external tendons and dry joints have already been constructed. Substantial economic and construction time savings have been indicated for this type of construction. However, analytical evaluation of their behavior is needed before additional construction proceeds.

An exact analysis of segmental bridges with external tendons is extremely difficult. It requires finding stress and displacement functions that satisfy the equilibrium equations, the constitutive relationships, and the compatibility conditions at every point in the system. An approximate analysis based upon an assumed form of the solution is satisfactory. However, finding suitable displacement or stress functions to approximate the whole domain of an externally prestressed segmental bridge is complicated. This may be simplified by discretization of the system into a finite number of components whose behavior can be approximated, and then assembling the original system from its components for analysis. This is the finite element approach whose results converge to the exact solution as the mesh of elements used becomes finer.

The primary objective of this report is to develop a finite element formulation suitable for evaluating the response of segmental bridges with external tendons subject

to service and overloads. The formulation is verified by comparing its results with classical solutions and actual behavior using linear and nonlinear material solution procedures. The analysis technique is also applied to an actual bridge model designed for physical testing.

In the following chapter, the finite element modeling and formulation for segmental bridges with external tendons is developed. The nonlinear solution procedures are discussed in chapter three. Specific characteristics of the formulation are verified in chapter four. In chapter five a complete experimental bridge model is analyzed. In the final chapter the conclusions and summary of the work is given.

2. FINITE ELEMENT FORMULATION

A segmental bridge with external tendons is modeled with three types of finite elements. A one-dimensional beam element for the segments, a joint element that transmits forces between segments, and a tendon element connected to the segments by rigid diaphragms. Figure 2.1 illustrates a simple bridge span of two segments, modeled with four beam elements, three tendon elements, and one joint element.

This chapter presents the formulation of the three element types.

2.1 Beam Element

The segments are modeled by a one dimensional beam element including axial and flexural deformations. The beam cross section has a vertical axis of symmetry, and is only loaded along that axis, so torsional behavior is neglected. The element includes nonlinear material properties. Small deflections of the beam are assumed in the formulation, and time dependent effects are neglected.

Figure 2.2 shows the beam element under consideration. The horizontal and vertical displacements of the beam, $u(x, y)$ and $v(x, y)$ respectively, are:

$$\begin{cases} u(x, y) = u_o(x, y) + \Delta u(x, y) \\ v(x, y) = v_o(x, y) + \Delta v(x, y) \end{cases} \quad (2.1)$$

in which $u_o(x, y)$ and $v_o(x, y) = v_o(x)$ are the current displacements, and $\Delta u(x, y)$ and $\Delta v(x, y)$ are the displacement increments defined as follows:

$$\begin{cases} \Delta u(x, y) = -\Delta u_a(x) + y \frac{d}{dx} [\Delta v(x)] \\ \Delta v(x, y) = \Delta v(x) \end{cases} \quad (2.2)$$

where $\Delta u_a(x)$ and $\Delta v(x)$ are the horizontal and vertical displacement increments along the reference axis of the element. The sign convention assumes that compressive distortions are positive.

The displacement field is approximated by a discrete set of degrees-of-freedom at the two nodes of the element. At each node there are two translations

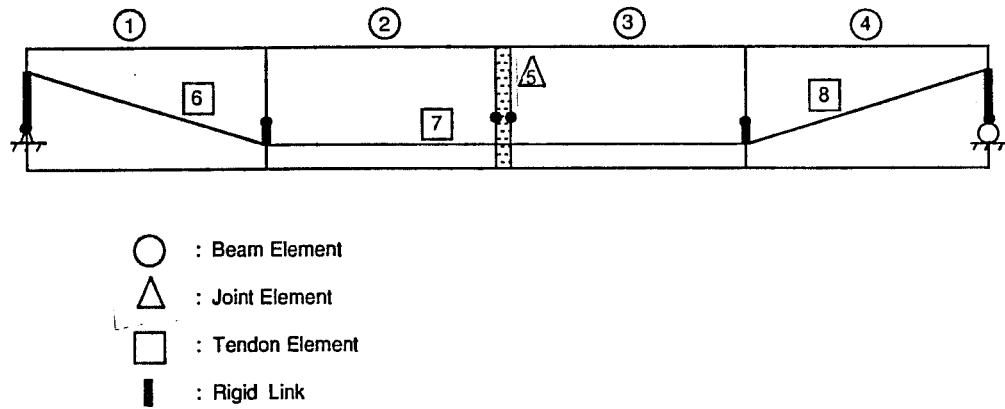


Fig. 2.1 Finite element model for a simple-span, segmental bridge with external tendons

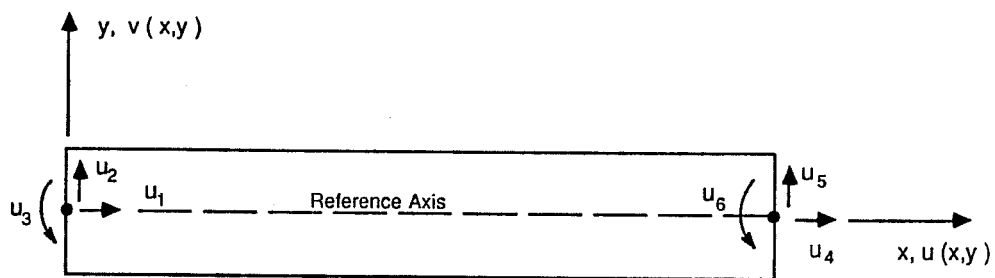


Fig. 2.2 Beam element model

and one rotation (Fig. 2.2), such that the change in displacements along the axis of the element are given by:

$$\begin{Bmatrix} -\Delta u_a(x) \\ \Delta v(x) \end{Bmatrix} = \underline{\underline{N}} \cdot \Delta \underline{\underline{U}} \quad (2.3)$$

where

$$\underline{\underline{N}} = \begin{bmatrix} -N_{1u}(x) & 0 & 0 & -N_{2u}(x) & 0 & 0 \\ 0 & N_{1v}(x) & N_{2v}(x) & 0 & N_{3v}(x) & N_{4v}(x) \end{bmatrix} \quad (2.4)$$

in which $N_{iu}(x)$ are standard axial linear shape functions, and $N_{iv}(x)$ are standard flexural cubic shape functions, and

$$\Delta \underline{\underline{U}} = \begin{Bmatrix} \Delta u_1 \\ \Delta u_2 \\ \Delta u_3 \\ \Delta u_4 \\ \Delta u_5 \\ \Delta u_6 \end{Bmatrix} \quad (2.5)$$

Assuming plane sections remain plane during deformation, the longitudinal strain and curvature are:

$$\begin{cases} \epsilon(x, y) = \epsilon_o(x, y) + \Delta\epsilon(x, y) \\ \phi(x, y) = \phi_o(x, y) + \Delta\phi(x, y) \end{cases} \quad (2.6)$$

where $\epsilon_o(x, y)$ and $\phi_o(x, y)$ are the current longitudinal strain and curvature, and

$$\begin{aligned} \Delta\epsilon(x, y) &= \frac{d}{dx}[\Delta u(x, y)] \\ &= \frac{d}{dx}[-\Delta u_a(x)] + y \frac{d^2}{dx^2}[\Delta v(x)] \\ &= -\Delta\epsilon_a(x) + y\Delta\phi(x) \end{aligned} \quad (2.7a)$$

also

$$\begin{aligned} \Delta\phi(x, y) &= \frac{d^2}{dx^2}[\Delta v(x)] \\ &= \Delta\phi(x) \end{aligned} \quad (2.7b)$$

Therefore, Eqs 2.3 and 2.7 produce:

$$\begin{Bmatrix} -\Delta\epsilon_a(x) \\ \Delta\phi(x) \end{Bmatrix} = \underline{\underline{B}} \cdot \Delta \underline{\underline{U}} \quad (2.8)$$

where

$$\underline{\underline{B}} = \begin{bmatrix} \frac{-d}{dx} N_{1u}(x) & 0 & 0 & \frac{-d}{dx} N_{2u}(x) & 0 & 0 \\ 0 & \frac{d^2}{dx^2} N_{1v}(x) & \frac{d^2}{dx^2} N_{2v}(x) & 0 & \frac{d^2}{dx^2} N_{3v}(x) & \frac{d^2}{dx^2} N_{4v}(x) \end{bmatrix} \quad (2.9)$$

Stresses in the element can be obtained from strains from the constitutive relationships for the materials. Figure 2.3 shows typical uniaxial stress-strain relationships for concrete and steel.

The stresses in a material j , are:

$$\sigma_j(x, y) = \sigma_{j_o}(x, y) + \Delta\sigma_j(x, y) \quad (2.10)$$

where $\sigma_{j_o}(x, y)$ is the current stresses of material j , and

$$\Delta\sigma_j(x, y) = \frac{d\sigma_j(x, y)}{d\epsilon} \cdot \Delta\epsilon(x, y) \quad (2.11)$$

Internal forces on the element are obtained by integrating stresses in the NM materials over the cross section as follows:

$$\begin{cases} P(x) = \sum_{j=1}^{NM} \int_{A_j} \sigma_j(x, y) \cdot dA_j \\ M(x) = \sum_{j=1}^{NM} \int_{A_j} \sigma_j(x, y) \cdot y \cdot dA_j \end{cases} \quad (2.12)$$

where A_j is the cross-sectional area of material j . Substituting Eqs 2.10 and 2.11 into Eqs 2.12, they give:

$$\begin{cases} P(x) = P_o(x) + \Delta P(x) \\ M(x) = M_o(x) + \Delta M(x) \end{cases} \quad (2.13)$$

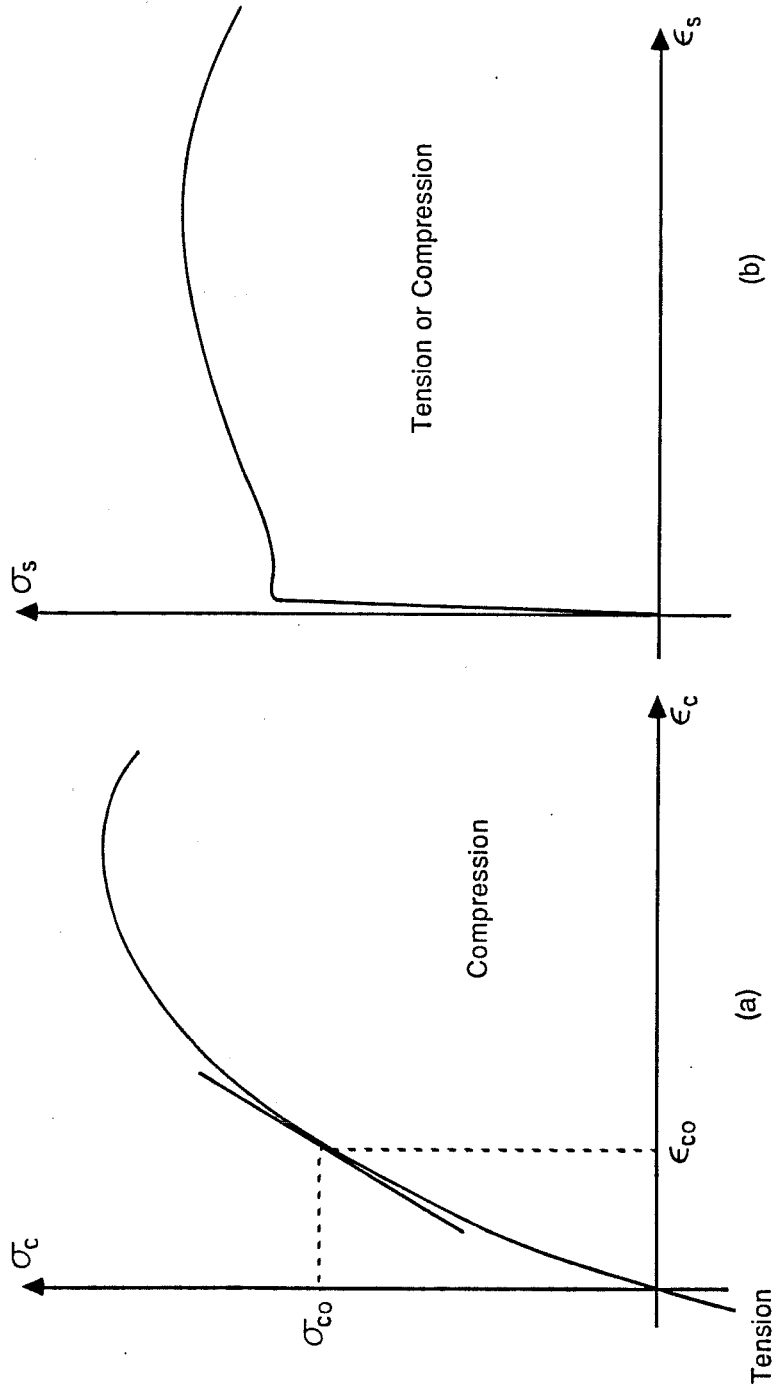


Fig. 2.3 Stress-strain relationships for (a) concrete and (b) reinforcing steel

where

$$\left\{ \begin{array}{l} P_o(x) = \sum_{j=1}^{NM} \int_{A_j} \sigma_{j_o}(x, y) \cdot dA_j \\ \Delta P(x) = \sum_{j=1}^{NM} \int_{A_j} \frac{d\sigma_j(x, y)}{d\epsilon} \cdot \Delta\epsilon(x, y) \cdot dA_j \\ M_o(x) = \sum_{j=1}^{NM} \int_{A_j} \sigma_{j_o}(x, y) \cdot y \cdot dA_j \\ \Delta M(x) = \sum_{j=1}^{NM} \int_{A_j} \frac{d\sigma_j(x, y)}{d\epsilon} \cdot \Delta\epsilon(x, y) \cdot y \cdot dA_j \end{array} \right. \quad (2.14)$$

To evaluate the integrals for internal forces, the beam cross section is divided into fibers in which the longitudinal strain and stress are constant. An example of a reinforced concrete cross section using a fiber model is shown in Fig. 2.4.

The internal force integrals are replaced by summation over N fibers, such that:

$$\left\{ \begin{array}{l} P_o(x) = \sum_{i=1}^N \sigma_{o_i}(x, y) \cdot A_i \\ \Delta P(x) = \sum_{i=1}^N \frac{d\sigma_i(x, y)}{d\epsilon} \cdot \Delta\epsilon(x, y) \cdot A_i \\ M_o(x) = \sum_{i=1}^N \sigma_{o_i}(x, y) \cdot y_i \cdot A_i \\ \Delta M(x) = \sum_{i=1}^N \frac{d\sigma_i(x, y)}{d\epsilon} \cdot \Delta\epsilon(x, y) \cdot y_i \cdot A_i \end{array} \right. \quad (2.15)$$

where it is not necessary to distinguish materials in the summations. The initial stress and tangent modulus, $\sigma_{o_i}(x, y)$ and $\frac{d\sigma_i}{d\epsilon}(x, y)$, respectively, are evaluated at each fiber from uniaxial stress-strain relationships for the corresponding material.

Substituting Eq 2.7a for $\Delta P(x)$ and $\Delta M(x)$ in Eq 2.15, gives:

$$\left\{ \begin{array}{l} \Delta P(x) \\ \Delta M(x) \end{array} \right\} = \underline{\underline{D}} \cdot \left\{ \begin{array}{l} -\Delta\epsilon_a(x) \\ \Delta\phi(x) \end{array} \right\} \quad (2.16)$$

where

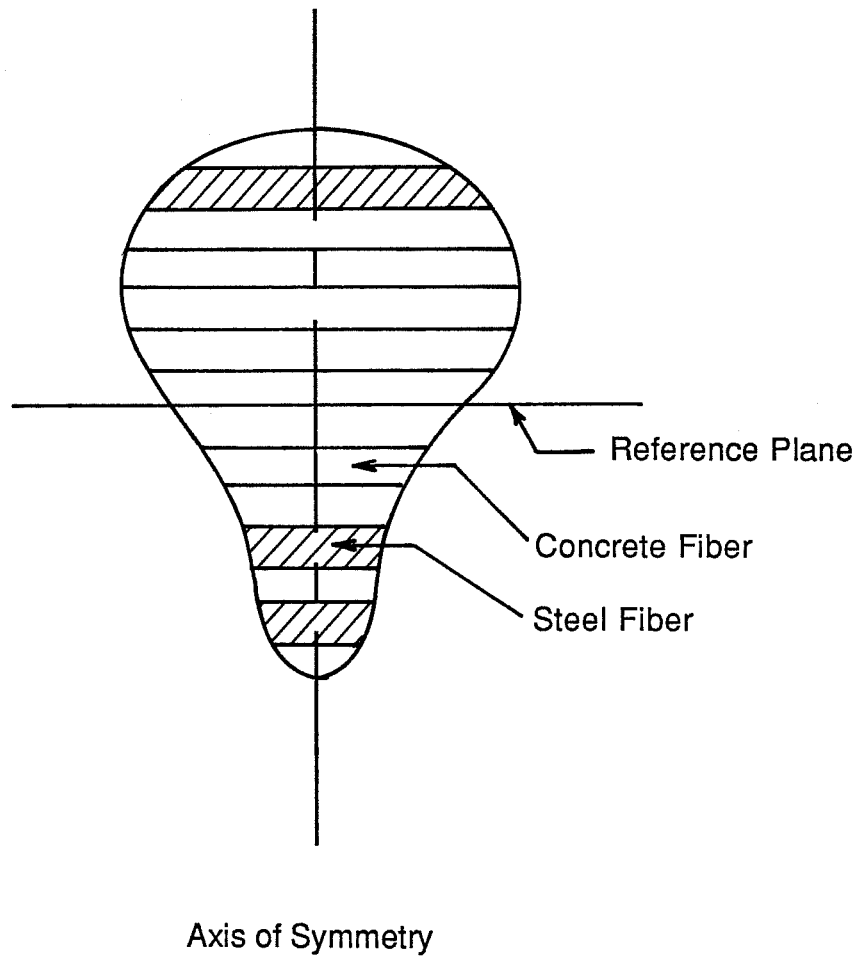


Fig. 2.4 Reinforced-concrete fiber cross section

$$\underline{\underline{D}} = \begin{bmatrix} \sum_{i=1}^N \frac{d\sigma_i(x,y)}{d\epsilon} \cdot A_i & \sum_{i=1}^N \frac{d\sigma_i(x,y)}{d\epsilon} \cdot y_i \cdot A_i \\ \sum_{i=1}^N \frac{d\sigma_i(x,y)}{d\epsilon} \cdot y_i \cdot A_i & \sum_{i=1}^N \frac{d\sigma_i(x,y)}{d\epsilon} \cdot y_i^2 \cdot A_i \end{bmatrix} \quad (2.17)$$

Using the strain-displacement relationships in Eq 2.8, Eq 2.16 becomes:

$$\begin{Bmatrix} \Delta P(x) \\ \Delta M(x) \end{Bmatrix} = \underline{\underline{D}} \cdot \underline{\underline{B}} \cdot \Delta U \quad (2.18)$$

Applying the principle of virtual work, the internal forces are related to external forces as follows:

$$\int_0^L \langle -\delta\epsilon_a(x) \quad \delta\phi(x) \rangle \begin{Bmatrix} P(x) \\ M(x) \end{Bmatrix} dx = \int_0^L \delta v(x) \cdot q(x) \cdot dx \quad (2.19)$$

where L is the length of the element, $\delta\epsilon_a(x)$, $\delta\phi(x)$, and $\delta v(x)$ are small virtual axial strain, curvature, and vertical displacement respectively, and $q(x)$ is the external load on the element, and is defined as:

$$q(x) = q_o(x) + \Delta q(x) \quad (2.20)$$

in which $q_o(x)$ is the current load, and $\Delta q(x)$ is the increment of load. Assuming the virtual displacement and strain fields have the same functional form as the real fields, then

$$\delta v(x) = \underline{\underline{N}}_v \cdot \delta U \quad (2.21a)$$

and

$$\begin{Bmatrix} -\delta\epsilon_a(x) \\ \delta\phi(x) \end{Bmatrix} = \underline{\underline{B}} \cdot \delta U \quad (2.21b)$$

in which

$$\underline{\underline{N}}_v = \langle 0 \quad N_{1v}(x) \quad N_{2v}(x) \quad 0 \quad N_{3v}(x) \quad N_{4v}(x) \rangle$$

These functions follow from Eqs 2.3 and 2.8, respectively.

Substituting Eqs 2.13, 2.20, 2.21 into Eq 2.19, and using Eq 2.18 gives the equilibrium equations for an element:

$$\underline{\underline{K}}_t \cdot \underline{\underline{\Delta U}} = (-\underline{\underline{F}}_o + \underline{\underline{P}}_{oe}) + \underline{\underline{\Delta P}}_e \quad (2.22)$$

where

$$\underline{\underline{K}}_t = \int_o^L \underline{\underline{B}}^T \cdot \underline{\underline{D}} \cdot \underline{\underline{B}} \cdot dx \quad (2.23a)$$

is the element tangent stiffness matrix,

$$\underline{\underline{F}}_o = \int_o^L \underline{\underline{B}}^T \cdot \left\{ \begin{array}{c} P_o(x) \\ M_o(x) \end{array} \right\} dx \quad (2.23b)$$

is the current internal nodal-force vector,

$$\underline{\underline{P}}_{oe} = \int_o^L \underline{\underline{N}}_v^T \cdot q_o(x) \cdot dx \quad (2.23c)$$

is the current external nodal-force vector, and

$$\underline{\underline{\Delta P}}_e = \int_o^L \underline{\underline{N}}_v^T \cdot \Delta q(x) \cdot dx \quad (2.23d)$$

is the incremental nodal-force vector. Because the vector $(-\underline{\underline{F}}_o + \underline{\underline{P}}_{oe})$ is zero if the previous increment reaches equilibrium, then

$$\underline{\underline{K}}_t \cdot \underline{\underline{\Delta U}} = \underline{\underline{\Delta P}}_e \quad (2.24)$$

The integrals in Eq 2.23 are evaluated numerically using gaussian quadrature.^{2,5} The corresponding expressions for numerical integration of these terms are:

$$\underline{\underline{K}}_t = \sum_{k=1}^M W_k \cdot \underline{\underline{B}}^T(\zeta_k) \cdot \underline{\underline{D}}(\zeta_k) \cdot \underline{\underline{B}}(\zeta_k) \cdot |J(\zeta_k)| \quad (2.25a)$$

$$\underline{\underline{F}}_o = \sum_{k=1}^M W_k \cdot \underline{\underline{B}}^T(\zeta_k) \cdot \left\{ \begin{matrix} P_o(\zeta_k) \\ M_o(\zeta_k) \end{matrix} \right\} \cdot |J(\zeta_k)| \quad (2.25b)$$

$$\underline{\underline{P}}_{oe} = \sum_{k=1}^M W_k \cdot \underline{\underline{N}}_v^T(\zeta_k) \cdot q_o(\zeta_k) \cdot |J(\zeta_k)| \quad (2.25c)$$

$$\underline{\underline{\Delta P}}_e = \sum_{k=1}^M W_k \cdot \underline{\underline{N}}_v^T(\zeta_k) \cdot \Delta q(\zeta_k) \cdot |J(\zeta_k)| \quad (2.25d)$$

In these expressions, ζ is a dimensionless variable with its origin at the center of the range of integration, ζ_k and W_k are the location and weighting factor of point k relative to the center, and M is the number of points at which the summations are to be evaluated. Also $|J(\zeta_k)| = dx/d\zeta$ is the Jacobian for the transformation of coordinates.

The number of integration points, M , should be selected for accurate numerical integration of the integrands. The order of the polynomials in Eq 2.25 depends on the shape functions, and the variation of stresses and applied loads along the element. For axial-linear and flexural-cubic shape functions, and for typical materials and loads, the integrals in Eq 2.28 can be integrated with satisfactory accuracy using three integration points.

2.2 External Tendon Element

The external tendon element is a one-dimensional axial element connected to beam elements by rigid links representing diaphragms. The element includes material nonlinearity of the tendon, but small deflections are assumed. Figure 2.5 shows the external tendon element. Important geometric information is:

$$\begin{cases} Lp = [(L + g_1 - g_2)^2 + (d + e_2 - e_1)^2]^{1/2} \\ \cos \theta = (L + g_1 - g_2)/Lp \\ \sin \theta = (d + e_2 - e_1)/Lp \end{cases} \quad (2.26)$$

The axial displacement of the tendon can be defined as:

$$u(x) = u_o(x) + \Delta u(x) \quad (2.27)$$

where $u_o(x)$ is the current displacement. The quantity $\Delta u(x)$ is the change in displacement, which is related to the end displacements of the tendons, $\Delta u'_1$ and $\Delta u'_2$, by axial shape functions, (Fig. 2.6):

$$\Delta u(x) = \underline{N} \cdot \begin{Bmatrix} \Delta u'_1 \\ \Delta u'_2 \end{Bmatrix} \quad (2.28)$$

where

$$\underline{N} = \left\langle 1 - \frac{x}{L}, \frac{x}{L} \right\rangle$$

Figure 2.6 also shows the relationship between u'_1 , u'_2 and the displacements at the nodes of the element. The incremental relationship is:

$$\begin{Bmatrix} \Delta u'_1 \\ \Delta u'_2 \end{Bmatrix} = \underline{A} \cdot \Delta U \quad (2.29)$$

where

$$\underline{A} = \begin{bmatrix} C & S & -\beta_1 & 0 & 0 & 0 \\ 0 & 0 & 0 & C & S & -\beta_2 \end{bmatrix} \quad (2.30)$$

in which

$$\begin{cases} C & = \cos \theta \\ S & = \sin \theta \\ \beta_1 & = e_1 C + g_1 S \\ \beta_2 & = e_2 C + g_2 S \end{cases}$$

Substituting Eq 2.29 into Eq 2.28, gives:

$$\Delta u(x) = \underline{N} \cdot \underline{A} \cdot \Delta U \quad (2.31)$$

The strain of the tendon is constant and is given by:

$$\epsilon = \epsilon_o + \Delta \epsilon \quad (2.32)$$

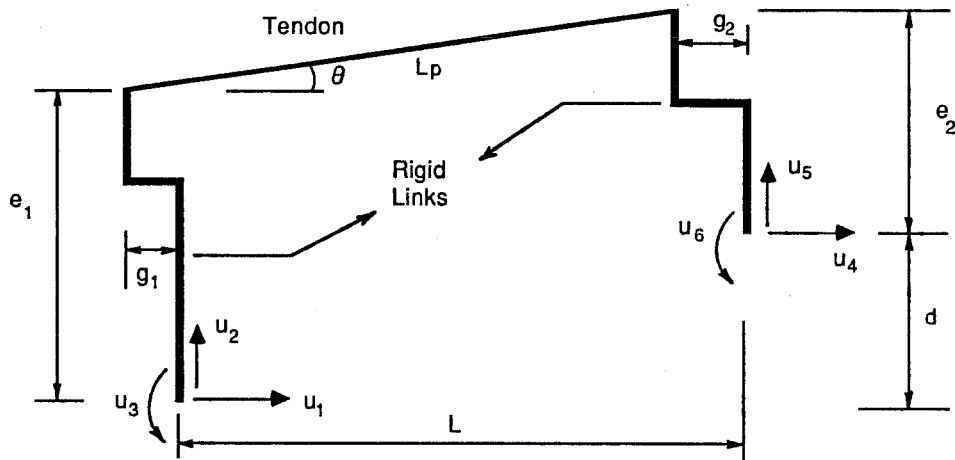


Fig. 2.5 External tendon element model

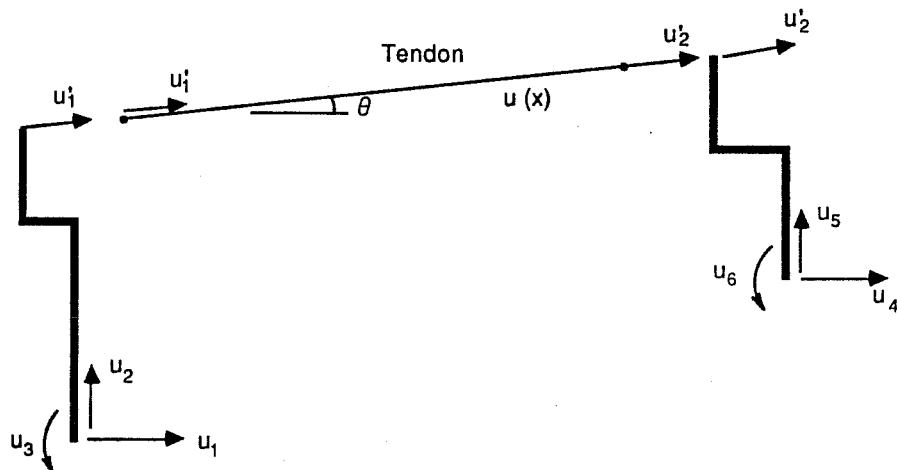


Fig. 2.6 Compatibility relationships of the tendon element

where ϵ_o is the original strain, and

$$\Delta\epsilon = \frac{d}{dx}[\Delta u(x)] \quad (2.33)$$

Using Eq 2.31, Eq 2.33 becomes:

$$\Delta\epsilon = \underline{\underline{B}} \cdot \Delta \tilde{U} \quad (2.34)$$

where

$$\underline{\underline{B}} = \frac{1}{Lp} \langle -C \quad -S \quad \beta_1 \quad C \quad S \quad -\beta_2 \rangle \quad (2.35)$$

The stress in the tendon is obtained from the constitutive relationship for the tendon material as a function of strain:

$$\sigma = \sigma_o + \Delta\sigma \quad (2.36)$$

σ_o is the original stress, and

$$\Delta\sigma = \frac{d\sigma}{d\epsilon} \cdot \Delta\epsilon \quad (2.37)$$

Thus, using Eq 2.34, The change in stress is:

$$\Delta\sigma = \frac{d\sigma}{d\epsilon} \cdot \underline{\underline{B}} \cdot \Delta \tilde{U} \quad (2.38)$$

The principle of virtual work gives:

$$\int_{V_p} \delta\epsilon^T \cdot \sigma \cdot dV_p = \delta U^T \cdot (\tilde{P}_{oe} + \Delta \tilde{P}_e) \quad (2.39)$$

in which V_p is the volume of the tendon, \tilde{P}_{oe} and $\Delta \tilde{P}_e$ are the current and incremental external nodal loads respectively, and $\delta\epsilon^T$ and δU^T are virtual axial strain and nodal displacements respectively, such that

$$\delta\epsilon^T = \delta U^T \cdot \underline{\underline{B}}^T \quad (2.40)$$

Using Eqs 2.36, 2.38, and 2.40 in Eq 2.39 gives the equilibrium equations for a tendon element:

$$\underline{\underline{K}}_t \cdot \Delta \tilde{U} = (-\tilde{F}_o + \tilde{P}_{oe}) + \Delta \tilde{P}_e \quad (2.41)$$

where

$$\underline{\underline{K}}_t = A_p \int_0^{L_p} \underline{\underline{B}}^T \cdot \frac{d\sigma}{d\epsilon} \cdot \underline{\underline{B}} \cdot dx \quad (2.42a)$$

is the tangent stiffness matrix, and

$$\underline{\underline{F}}_o = A_p \int_0^{L_p} \underline{\underline{B}}^T \cdot \sigma_o \cdot dx \quad (2.42b)$$

is the current internal nodal force vector which includes initial prestress forces. A_p is the cross sectional area of the tendon.

Substituting Eq 2.35 into Eq 2.42a, gives the tangent stiffness matrix:

$$\underline{\underline{K}}_t = D_p \begin{bmatrix} C^2 & CS & -\beta_1 C & -C^2 & -CS & \beta_2 C \\ & S^2 & -\beta_1 S & -CS & -S^2 & \beta_2 S \\ & & \beta_1^2 & C\beta_1 & S\beta_1 & -\beta_1\beta_2 \\ \text{Symmetric} & & & C^2 & CS & -\beta_2 C \\ & & & & S^2 & -\beta_2 S \\ & & & & & \beta_2^2 \end{bmatrix} \quad (2.43)$$

in which

$$D_p = \frac{d\sigma}{d\epsilon} \frac{A_p}{L_p}$$

Also substituting Eq 2.35 into Eq 2.42b, gives the internal force vector:

$$\underline{\underline{F}}_o = A_p \sigma_o \begin{Bmatrix} -C \\ -S \\ \beta_1 \\ C \\ S \\ -\beta_2 \end{Bmatrix} \quad (2.44)$$

2.3 Joint Element

The joint element models the behavior of the joints between two adjacent girder segments. The joint cannot resist tensile stresses above a specified level (zero if no epoxy is used). The gap between the segments is represented by a function $g(y)$,

Fig. 2.7a, and the force-displacement relationship for the joint is shown in Fig. 2.7b. The assumptions on the behavior of the joints are: (1) plane sections remain plane, (2) no relative vertical deflection (no slipping), (3) small deflection of joint, and (4) infinite strength of joint.

The joint element has four degrees-of-freedom as shown in Fig. 2.8; a horizontal translation and a rotation on each side of the joint. No relative vertical deformation of the joint is allowed, so it is not necessary to include a vertical degree-of-freedom in the joint element. The vertical displacement is included by assembly of adjoint beam elements.

The gap in the joint can be represented as:

$$g(y) = g_o(y) + \Delta g(y) \quad (2.45)$$

where $g_o(y)$ is the current gap, and $\Delta g(y)$ is the increment gap, such that

$$\Delta g(y) = \underline{b} \cdot \Delta U \quad (2.46)$$

where

$$\underline{b} = \langle 1 \quad -y \quad -1 \quad y \rangle$$

The model assumes that no epoxy is used, so the incremental force-displacement relationship is:

$$\Delta f(y) = \begin{cases} 0 & \text{for } g(y) < 0 \\ k \cdot \underline{b} \cdot \Delta U & \text{for } g(y) \geq 0 \end{cases} \quad (2.47)$$

in which k is the stiffness, and $\Delta f(y)$ is the increment force per unit depth of the joint. The value of k should be large compared to the axial stiffness of the beam, but not so large as to lead to ill-conditioning of the assembled structural stiffness matrix. The accumulated force is:

$$f(y) = f_o(y) + \Delta f(y) \quad (2.48)$$

with $f_o(y)$ as the current force per unit depth.

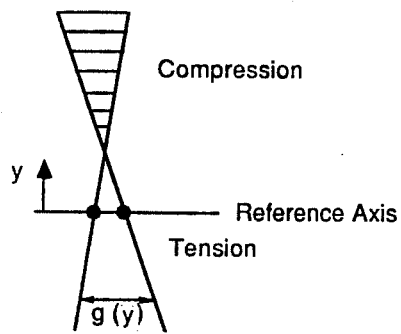


Fig. 2.7a Gap between segments

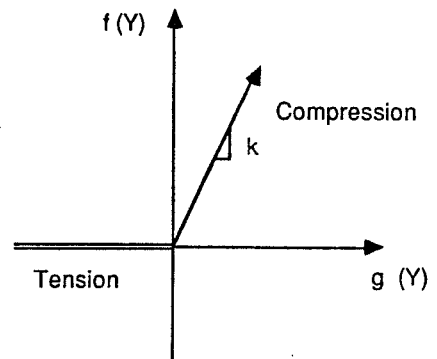


Fig. 2.7b Force-displacement relationship of the joint

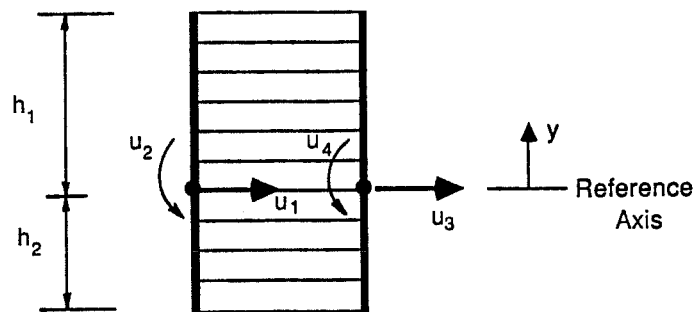


Fig. 2.8 Joint element model

The principle of virtual displacement for the joint element gives:

$$\int_{\Gamma_c} \delta_g^T(\mathbf{y}) \cdot \mathbf{f}(\mathbf{y}) \cdot d\mathbf{y} = \delta \tilde{U}^T \cdot (\tilde{P}_{oe} + \Delta \tilde{P}_e) \quad (2.49)$$

in which Γ_c is the depth of contact in the joint, and \tilde{P}_{oe} and $\Delta \tilde{P}_e$ are the original and increment forces on the element. The resulting equilibrium equation is:

$$\underline{\underline{K}}_t \cdot \Delta \tilde{U} = (-\tilde{F}_o + \tilde{P}_{oe}) + \Delta \tilde{P}_e \quad (2.50)$$

where

$$\underline{\underline{K}}_t = \int_{\Gamma_c} \underline{\underline{b}}^T \cdot k \cdot \underline{\underline{b}} \cdot d\mathbf{y} \quad (2.51a)$$

is the stiffness matrix, and

$$\tilde{F}_o = \int_{\Gamma_c} \underline{\underline{b}}^T \cdot \mathbf{f}_o(\mathbf{y}) \cdot d\mathbf{y} \quad (2.51b)$$

is the current internal force vector.

The area of contact is the part of the joint where $g(\mathbf{y}) \geq o$. The ordinate of the point where $g(\mathbf{y}) = 0$ is y_c , and it is calculated from Eq 2.46:

$$y_c = (u_1 - u_3)/(u_2 - u_4) \quad (2.52)$$

If $y_c \leq -h_2$ or $y_c \geq h_1$, where h_1 and h_2 are the distances to the extreme fibers of the joint from the nodes, the joint is all in tension or all in compression. If $-h_2 \leq y_c \leq h_1$, the joint is partly in tension and partly in compression. The four states of the element are given in Fig. 2.9, where a and b are the lower and upper limits of Γ_c .

Substituting the value of $\underline{\underline{b}}$ into Eq 2.51a, gives the stiffness matrix:

$$\underline{\underline{K}}_t = k \begin{bmatrix} I_1 & -I_2 & -I_1 & I_2 \\ & I_3 & I_2 & -I_3 \\ & & I_1 & -I_2 \\ & & & I_3 \end{bmatrix} \quad (2.53)$$

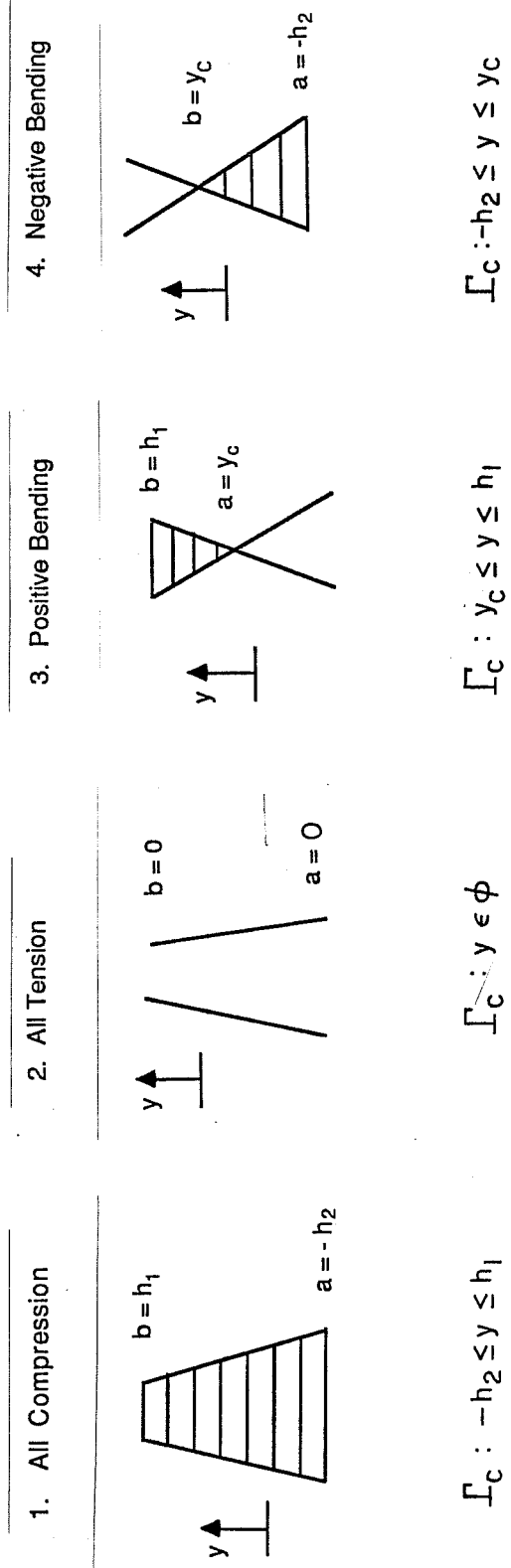


Fig. 2.9 Four states of the joint element

in which

$$I_n = \frac{1}{n}(b^n - a^n) \quad \text{with} \quad n = 1, 2, 3.$$

Also Eq 2.51b, using the same functional form of Eq 2.47 for $f_o(y)$, gives the expression for the internal force vector:

$$\tilde{F}_o = k \begin{Bmatrix} I_1 \cdot u_d - I_2 \cdot \theta_d \\ -I_2 \cdot u_d + I_3 \cdot \theta_d \\ -I_1 \cdot u_d + I_2 \cdot \theta_d \\ I_2 \cdot u_d - I_3 \cdot \theta_d \end{Bmatrix} \quad (2.54)$$

with $u_d = u_1 - u_3$ and $\theta_d = u_2 - u_4$.

The formulation of the joint assumes infinite strength, so a separate calculation for failure at joints is needed. For reinforced concrete segments, this must be accounted for in the analysis by considering the nominal strength of the material in the joint.

3. SOLUTION PROCEDURE

The element formulations presented in chapter two are used in a nonlinear solution procedure for analysis of external prestressed segmental bridges. An incremental solution with suitable small load increments is appropriate for convergence up to failure of the structure. The Newton-Raphson or Modified Newton-Raphson iteration procedures are used to obtain equilibrium convergence for each load increment. The computational steps for these procedures require three major steps: (1) linearization, (2) equation solution, and (3) state determination.

The nonlinear equilibrium equations representing the structure discretized with beam, tendon, and joint elements are:

$$\tilde{F}(\tilde{U}) = \tilde{P} \quad (3.1)$$

where \tilde{F} and \tilde{P} are the internal and external nodal load vectors. The solution of Eq 3.1 requires solving linearized forms of the equilibrium equations until convergence is reached.

In the Newton-Raphson procedure the tangent stiffness matrix is reformed at every step.⁶ The linearized equations are:

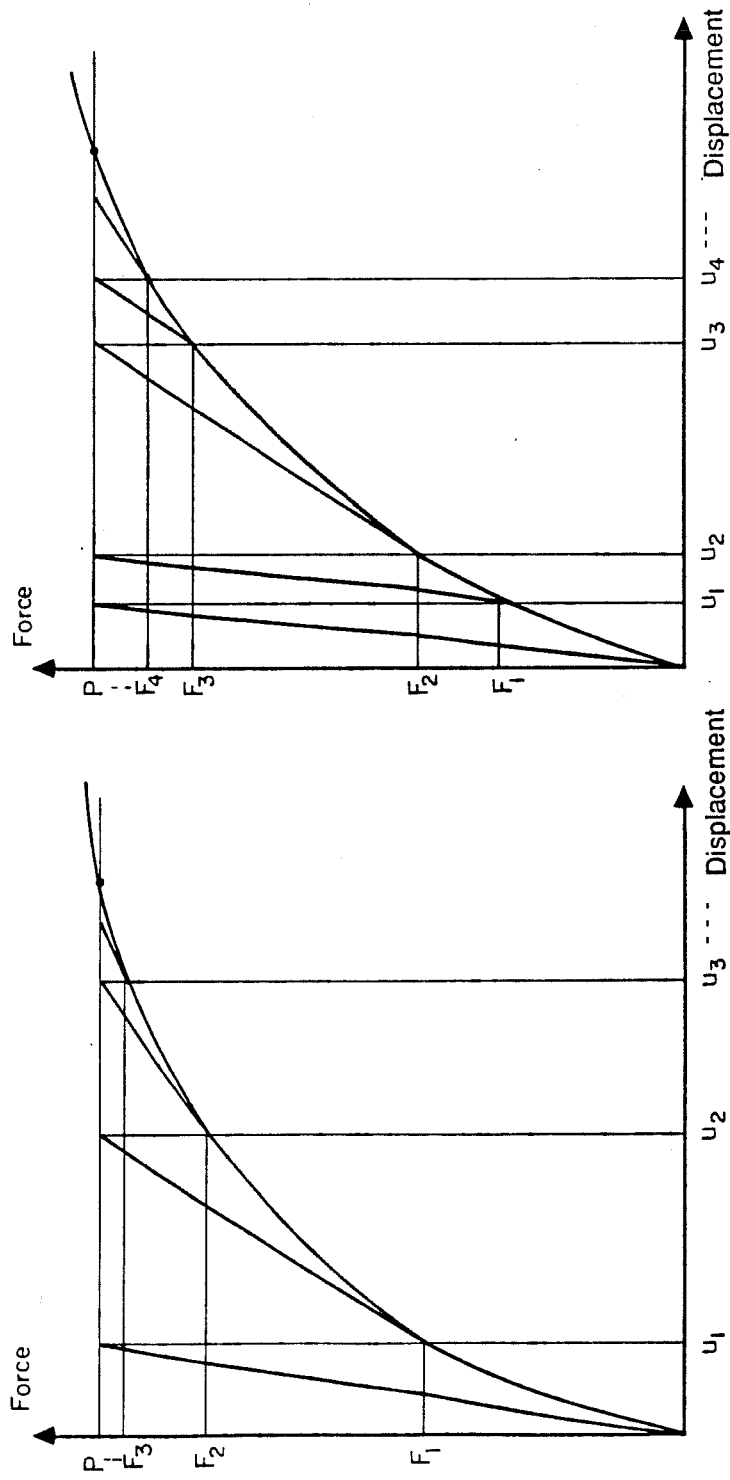
$$\underline{K}_t(\tilde{U}_n) \cdot \Delta \tilde{U}_n = \tilde{P} - \tilde{F}_n(\tilde{U}_n) \quad (3.2)$$

with

$$\tilde{U}_{n+1} = \tilde{U}_n + \Delta \tilde{U}_n$$

where the subscript n refers to the iteration number. Convergence is based on the norm of the unbalanced load vector on the right hand-side of Eq 3.2, and the norm of $\Delta \tilde{U}$, such that both are less than a specified tolerance. The iterative procedure is illustrated schematically in Fig. 3.1a for a problem with one degree of freedom.

In the Modified Newton-Raphson procedure, the tangent stiffness matrix is reformed only after several iterations. This is clearly more economical at each iteration but the convergence is slower. Figure 3.1b illustrates this method where \underline{K}_t is reformed every two iterations.



(a)

(b)

Fig. 3.1 Iteration methods: (a) Newton-Raphson iteration and (b) modified Newton-Raphson iteration (K_2 is reformed every two iterations.)

The computational steps involved in these procedures are now discussed as they relate to the formulation of the previous chapter.

3.1 Linearization

In this phase the tangent stiffness matrix, $\underline{K}_t(U_n)$, of the structure is assembled from the element stiffness matrices. Equations 2.25a, 2.43, and 2.53 give the formulation of the beam, tendon and joint element stiffness matrices, respectively.

3.2 Equation Solution

This step requires solution of the linearized equilibrium equations, Eq 3.2, for $\Delta \underline{U}_n$. This is optimally accomplished using gaussian elimination implemented by the Crout algorithm.^{2,6} The assembled stiffness matrix is symmetric and banded. However, because external tendon elements connect two distant nodes, the nonzero profile of the matrix has long columns and rows, creating a large bandwidth. Storage of the coefficients within the nonzero profile of the upper triangular portion of the stiffness matrix by columns has definite advantages over a banded storage. It almost always requires less storage and computational effort, and the storage requirements are not severely affected by few long columns. This is the active column profile (skyline) procedure.

3.3 State Determination

After the solution for the displacement increments is obtained, the new state for the elements is required. This involves the computation of strains, stresses and the vector for internal forces, $\underline{F}_n(\underline{U}_n)$. A path dependent state determination is used to allow for the situation where strains do not increase monotonically.

In the path dependent state determination, stresses are computed at the end of each iteration based on the strain increment for that iteration. In contrast, with path independent state determination the stresses are computed for the accumulated strain increments at any iteration. For cases in which the strains increase monotonically during iteration, the results with the two types can be expected to be in close agreement, Fig. 3.2a. However, if the strains do not increase monotonically, path dependent state determination may give better results, Fig. 3.2b.¹

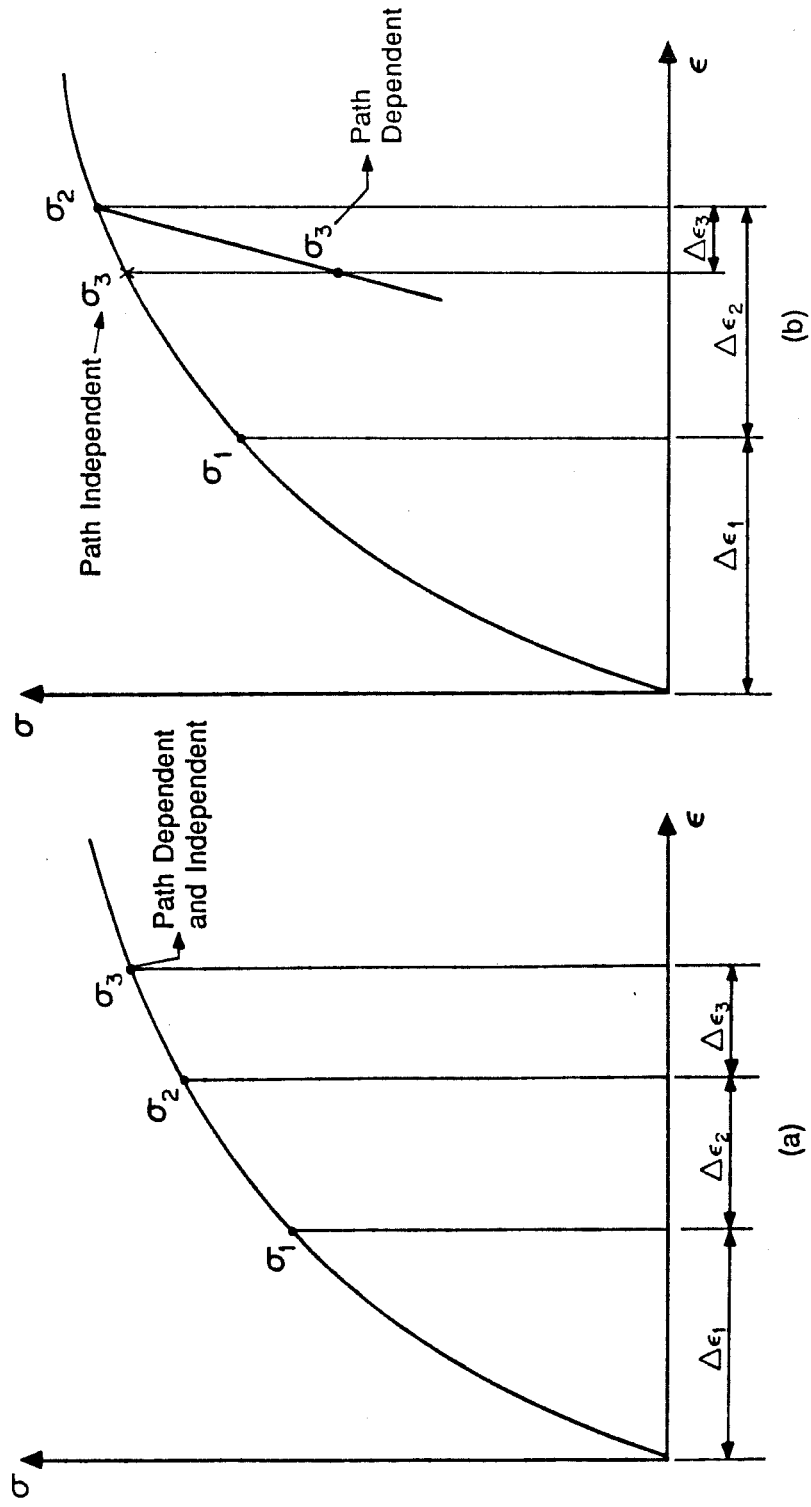


Fig. 3.2 Effect of path dependence: (a) monotonous loading (b) unloading

For the beam element, substitution of Eq 2.8 into Eq 2.7a gives the incremental strain for this iteration. The corresponding stress increment is computed from Eq 2.11 using the constitutive relationship for the materials. The accumulated stress up to any iteration is updated from Eq 2.10. $P_o(x)$ and $M_o(x)$ that correspond to the current stress $\sigma_o(x, y)$ are evaluated from Eq 2.15. Then, Eq 2.25b gives the current internal nodal forces in the beam element.

For the tendon element, Eq 2.34 gives the strain increment. The stress increment is determined from Eq 2.37, and the current stress, σ_o , is computed using Eq 2.36. The corresponding internal force vector is determined from Eq 2.44.

For the joint element, the increment gap and increment force per unit depth are computed from Eqs 2.46 and 2.47, respectively. Also, the current force per unit depth and the corresponding internal force vector for the element are determined from Eqs 2.48 and 2.54.

The internal resisting force vectors for each element are assembled to give $\tilde{F}_n(\tilde{U}_n)$, completing the state determination process at each iteration.

4. VERIFICATION OF FORMULATION

The finite element formulation in chapter two is verified here by comparing the analytical results with available solutions for several examples. Features unique to the formulation are tested, and the behavior of external prestressed bridges with and without joints are examined. Linear and nonlinear material behavior are considered in the examples.

Example 4.1: Number of Fibers in a Beam Cross Section

To evaluate the effect on the solution of the number of fibers used in a beam cross section, the composite beam shown in Fig. 4.1 is analyzed. The beam consists of two linear, elastic materials A and B, such that:

$$\begin{aligned}\text{Modulus of Elasticity of A} &= 1,000 \text{ ksi} \\ \text{Modulus of Elasticity of B} &= 20,000 \text{ ksi}.\end{aligned}$$

The cross section is modeled using 1, 2, 4, 8, and 16 fibers for material A, and 1 and 2 fibers for material B. The number of elements does not affect the solution because the beam has constant axial strain and curvature along the reference axis; two elements are used. The numerical results and exact solution are tabulated in Table 4.1. These results indicate rapid convergence, where ten fibers give an error of less than 1%, and should be satisfactory for practical analysis. An efficient fiber model should concentrate the fibers away from the neutral axis.

Example 4.2: Number of Elements in a Span

The simply supported beam of Fig. 4.2 is used to study the effect of the number of elements in a span. The materials are linear, elastic, where the moduli of elasticity are the same as in Ex 4.1, and the number of fibers is set at 16 and two for material A and B, respectively. The axial strain and curvature are linear functions on both sides of the load along the reference axis, which is not the neutral axis. The results of this example improve by increasing the number of elements because the formulation of the beam assumes constant axial strain. If the neutral axis had been selected as the reference axis, only two elements would be required for an

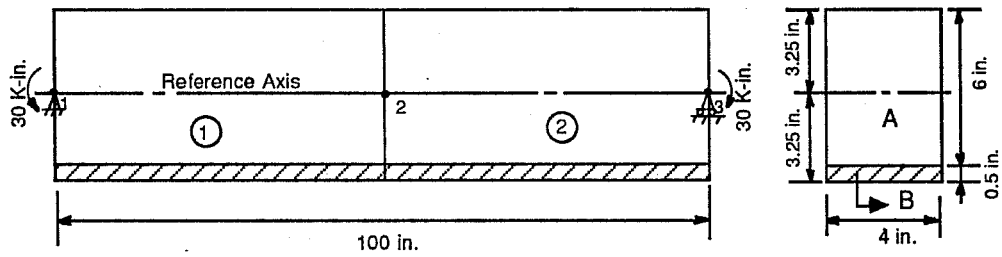


Fig. 4.1 Finite element layout for Example 4.1

Table 4.1 Results of Example 4.1

Number of A Fibers	Number of B Fibers	Horizontal Displacement of Point 3 (in.)	Rotation at Points 1 & 3 (\pm rad./in.)	Vertical Displacement of Point 2 (in.)	Percentage Error of Vert. Displacement
1	1	.03373	.009467	.2367	46.9
2	1	.02515	.007061	.1765	8.8
4	1	.02365	.006639	.1660	2.3
8	1	.02330	.006541	.1635	0.8
16	1	.02322	.006518	.1629	0.4
16	2	.02316	.006502	.1625	0.2
Exact Solution		.02309	.006486	.1622	—

exact solution. However, when nonlinear material behavior is allowed the location of the neutral axis changes, so it is important to assess the convergence as the number of elements increases. The structure is analyzed with 2,4,8 and 16 equal elements, and the results are shown in Table 4.2, in comparison to the exact solution. These results and the results from other examples indicate that the rate of convergence is a function of the degree of nonlinearity of the axial strain and curvature functions. Small elements should be used where these functions are highly nonlinear.

Example 4.3: Nonlinear Beam Behavior

In the following example, the model of a reinforced concrete beam includes a nonlinear stress-strain curve for concrete, and bilinear curves for passive steels. The beam is shown in Fig. 4.3. The material properties are:

Concrete:	$f'_c = 5.62 \text{ ksi}$	$f'_t = 0.611 \text{ ksi}$
	$\epsilon_{co} = 2.20 \times 10^{-3}$	$E_i = 4.87 \times 10^3 \text{ ksi}$
#4 Bars:	$f_{sy} = 50.1 \text{ ksi}$	$\epsilon_{su} = 0.2$
	$E_{s1} = 29.2 \times 10^3 \text{ ksi}$	$E_{s2} = 144 \text{ ksi}$
#9 Bars:	$f_{sy} = 80.1 \text{ ksi}$	$\epsilon_{su} = 0.139$
	$E_{s1} = 30.7 \times 10^3 \text{ ksi}$	$E_{s2} = 418 \text{ ksi}$

This beam is one of a series of beams tested by Bresler and Scordelis in 1961.⁴ The finite element model is similar to those used by previous researchers evaluating different analytical and numerical techniques. The load-deflection responses from the experimental results and from this analysis are given in Fig. 4.4. It shows that the finite element analysis approximates the actual behavior of the beam up to failure where the solution diverges at 80 K.

Examples 4.4 to 4.7: Effects of Tendons and Joints on Beam Behavior

The following examples consider the effects of external tendons and joints on the load-displacement behavior of a simply supported beam. Figure 4.5 shows the

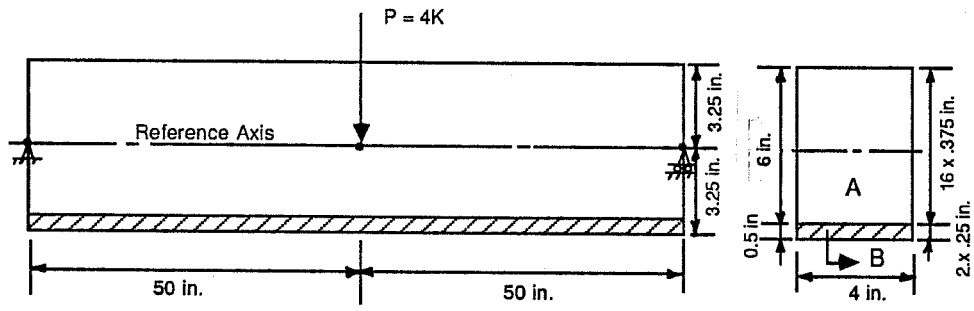


Fig. 4.2 Finite element layout for Example 4.2

Table 4.2 Results of Example 4.2

Number of Elements	Midspan Vertical Displacement (in.)	Percentage Error of Displacement
2	.3189	11.5
4	.3506	2.7
8	.3586	0.5
16	.3605	0.
Exact Solution	.3604	—

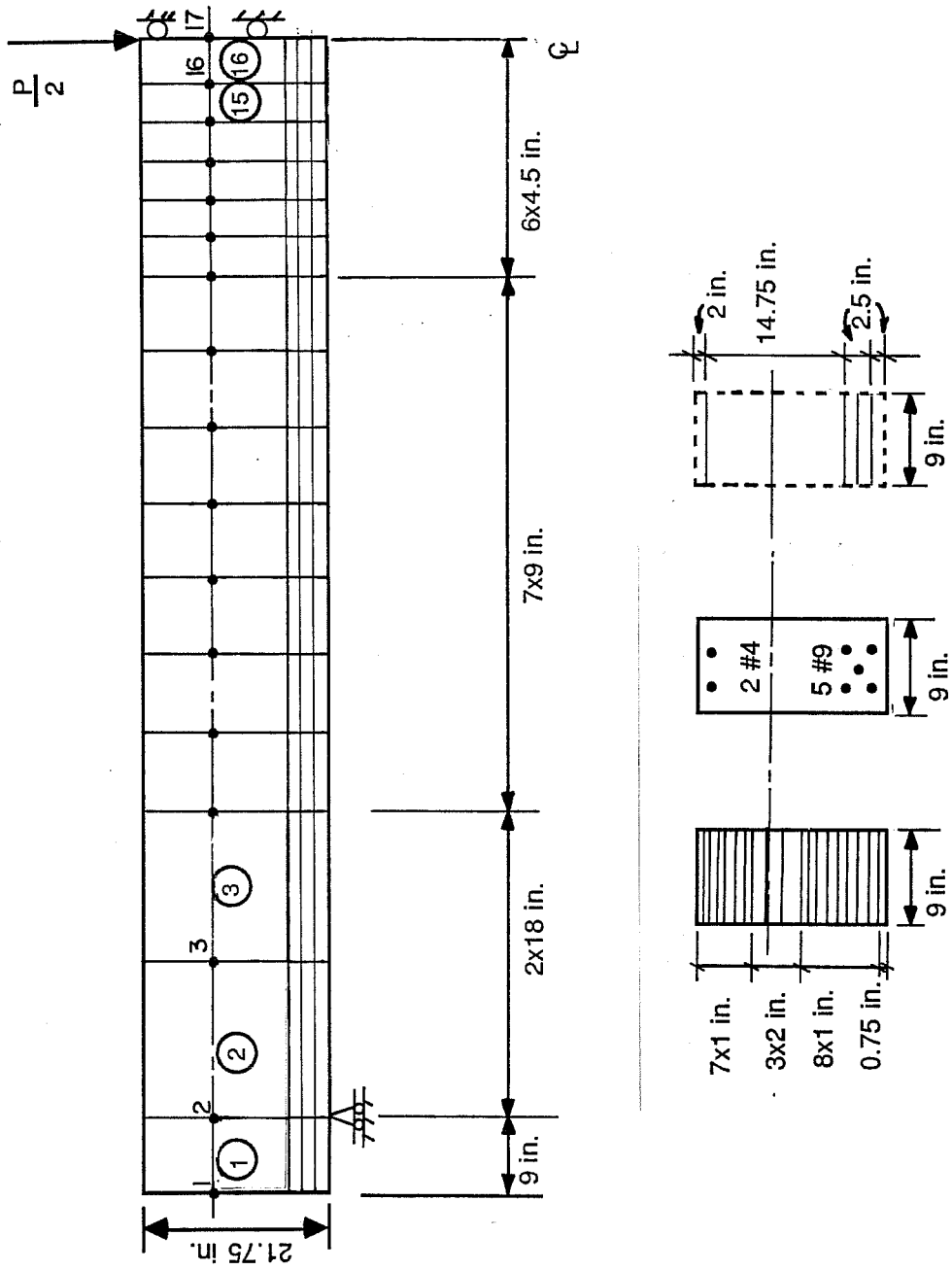


Fig. 4.3 Finite element model for verification of Example 4.3

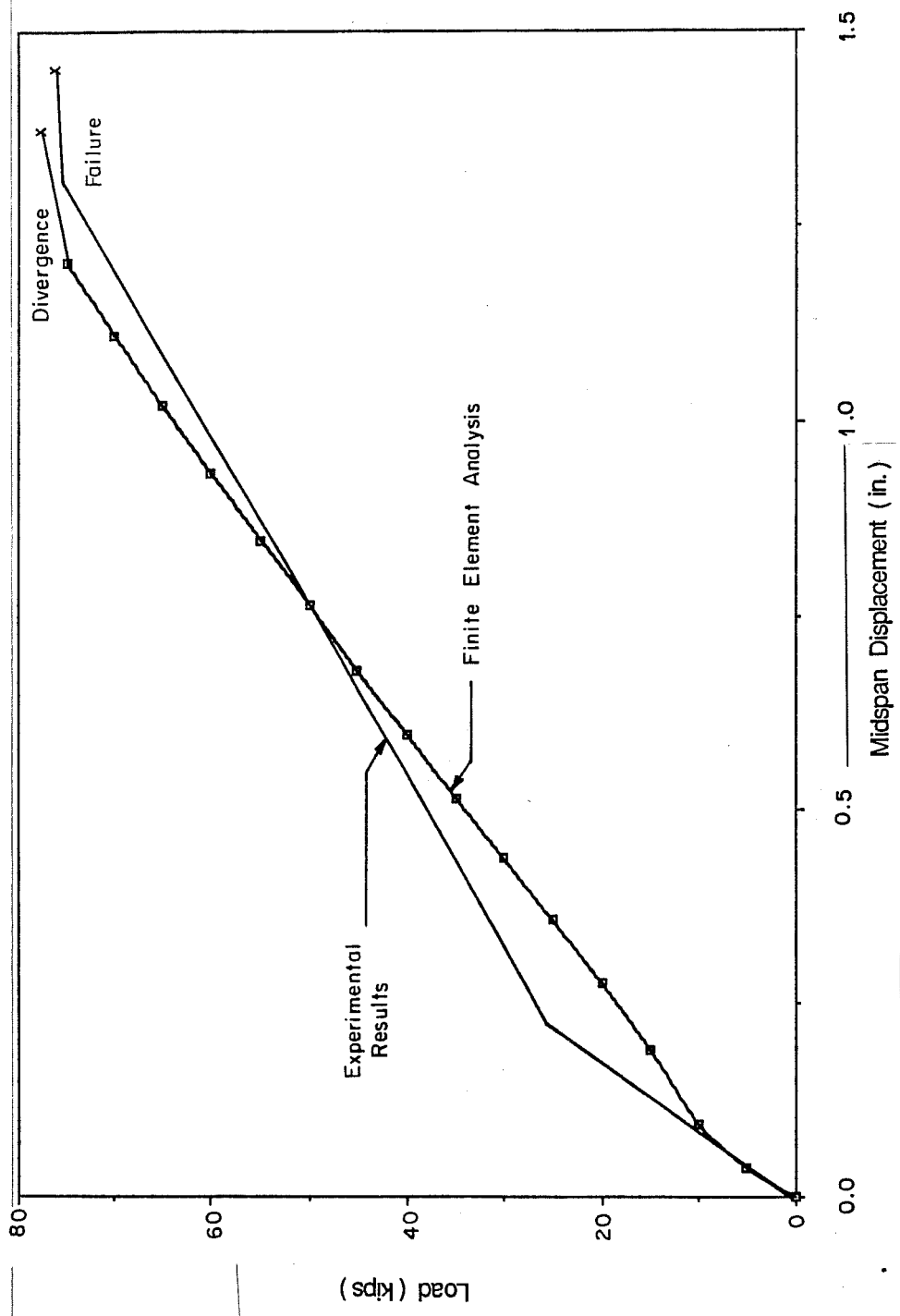


Fig. 4.4 Midspan load-displacement curves for Bresler-Scordelis (as in Ref. 3) experiment and finite element analysis of Example 4.3

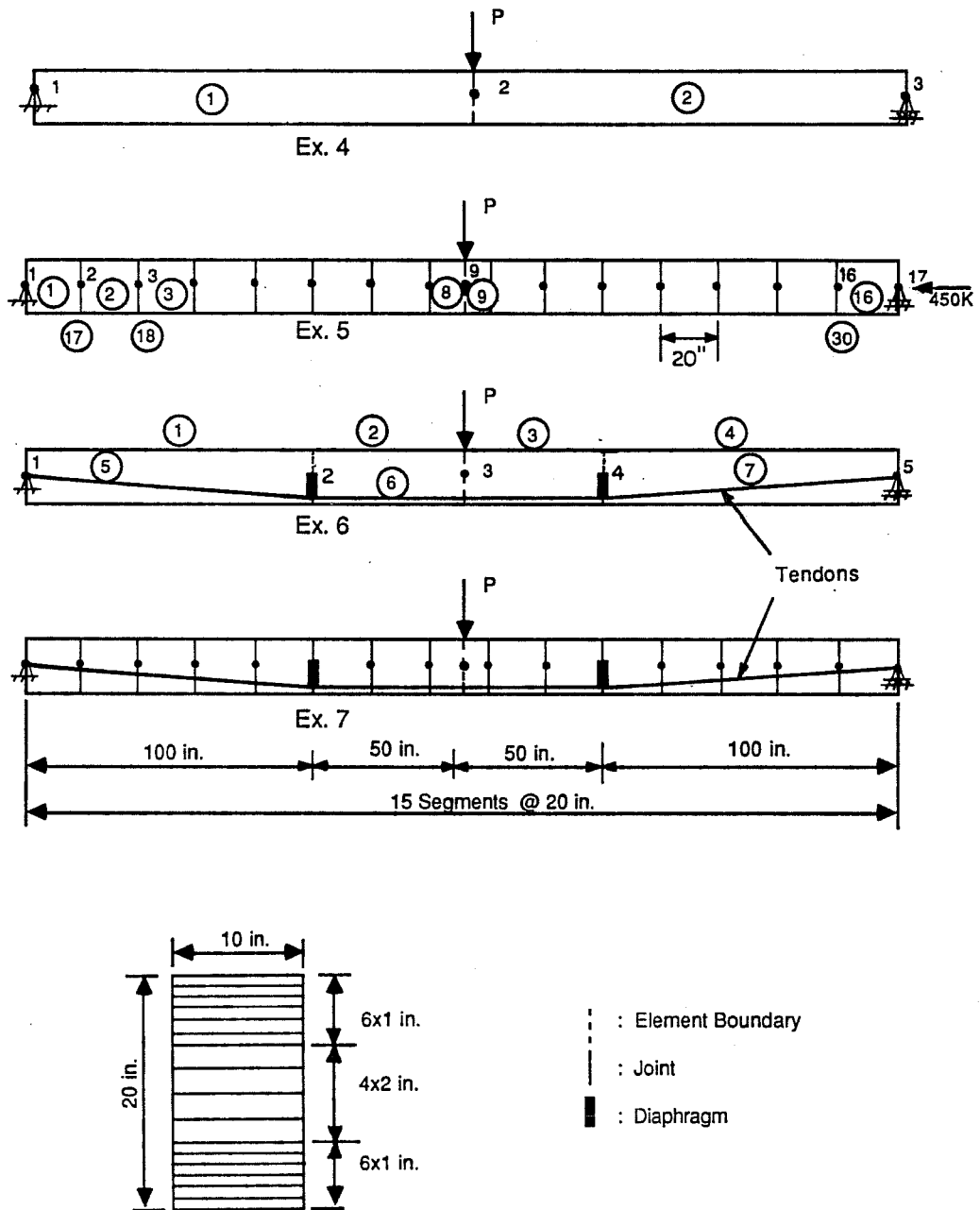


Fig. 4.5 Finite element model for Examples 4.4 to 4.7

four examples studied, having the same cross section. The beam and tendon materials are both linear and elastic with very high strength, where

Beam:	Modulus of Elasticity	= 4,000 <i>ksi</i>
Tendon:	Modulus of Elasticity	= 30,000 <i>ksi</i>
	Area	= 3 <i>in.</i> ²
	Initial Stress	= 450 <i>k.</i>

Example 4 is a one segment beam, while Ex 5 is formed of 15 segments held in equilibrium by an external axial load. Example 6 is the same as Ex 4 with a tendon, also Ex 7 is the same as Ex 5 with a tendon instead of the axial load. The force-displacement relationships of the four cases are tabulated and plotted in Table 4.3 and Fig. 4.6. Also, the fraction of the joint opening relative to the depth of the joint near the center is given.

Example 4 has a linear force-displacement relationship as expected. The same results can be determined using classical methods. Example 5 shows that the presence of the joints increases the flexibility of the structure after they start to open. The solution diverges at 70K where the axial force is not enough to maintain equilibrium. The force-displacement relationship in Ex 6 is linear. The external tendon causes an upward deflection that delays joint opening from the bottom, and increases the stiffness of the structure as verified by comparing the slope to that of Ex 4. Example 7, with joints and external tendons, shows that the effects of both types of elements are combined. Ultimately, the structure fails when the joints open to such an extent, that the increasing axial load in the tendon cannot match the corresponding increase in the beam's flexibility. Yielding of the tendons or crushing of the beam at the critical joints are other modes of failure that occur in similar structures with actual material strengths.

P (Kips)	Midspan Displacement (Positive Downward)(in.)					Diverges	Fraction of Joint Opening Near Center	
	Ex 4	Ex 5	Ex 6	Ex 7	Ex 5		Ex 7*	
0	0	0	-.9190	-.9358	0		0	-.55
10	0.2121	0.2142	-.7291	-.7363	0		0	-.26
20	0.4242	0.4284	-.5391	-.5432	0		0	0
30	0.6363	0.6429	-.3491	-.3514	0		.20	0
40	0.8484	0.8595	-.1591	-.1597	0		.43	0
50	1.061	1.085	0.0309	0.0320	0		.67	0
60	1.273	1.453	0.2209	0.2237	0		.90	0
70	1.485		0.4109	0.4155				.15
80	1.697		0.6008	0.6078				.34
90	1.909		0.7908	0.8019				.52
100	2.121		0.9808	1.001				.68
110	2.333		1.171	1.222				.82
120	2.545		1.361	1.494				.89
130	2.757		1.551	1.803				.92
140	2.969		1.741	2.137				.94
150	3.182		1.931	2.514				.94
160			2.121	2.924				.95
170			2.311	3.362				.95
180			2.501	3.825				.95
190			2.691	4.299				.96
200			2.881	4.776				.96

* Top joint opening is negative

Table 4.3 Midspan Load-Displacement and Joint Opening Fraction for Examples 4.4 to 4.7

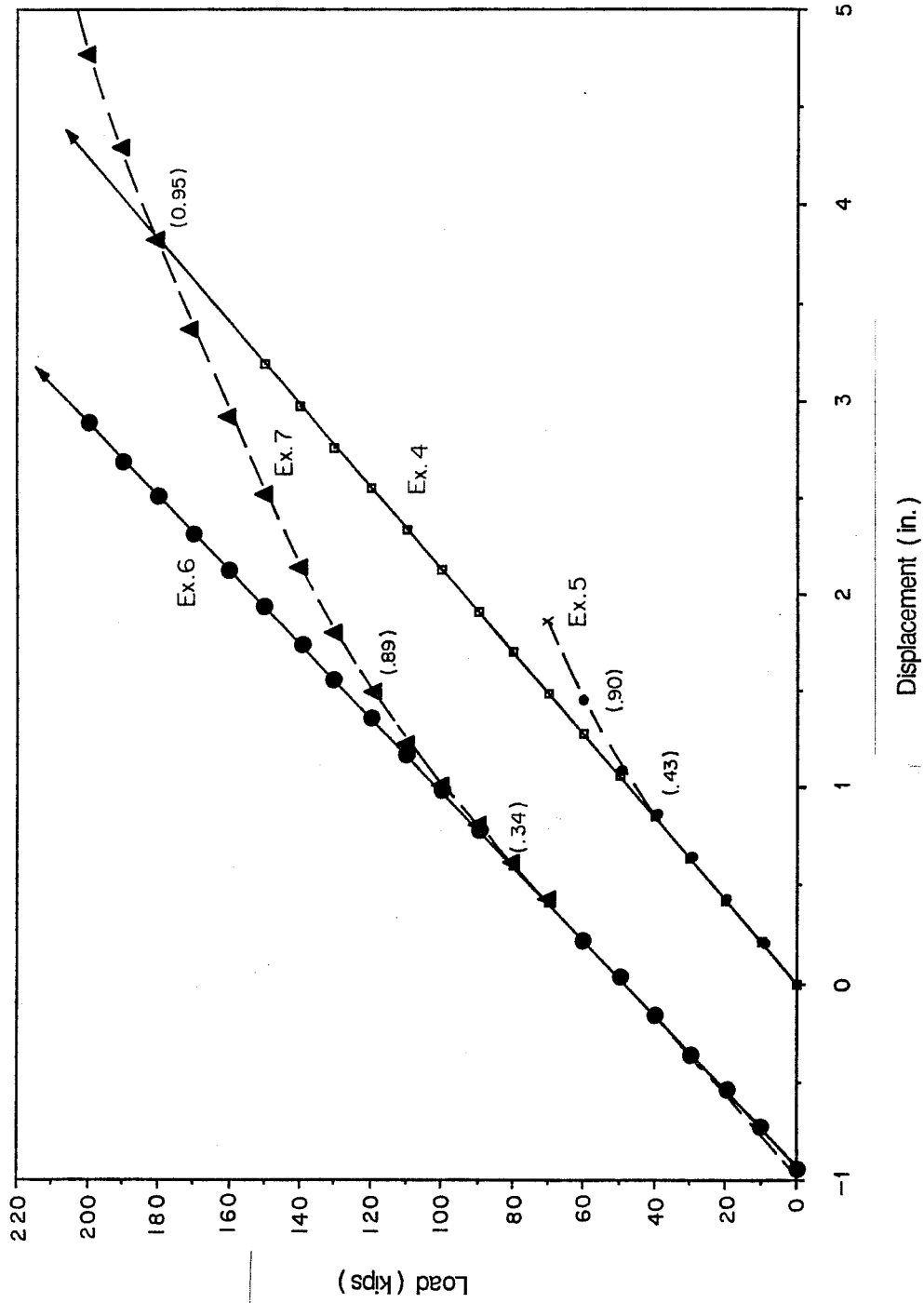


Fig. 4.6 Midspan load-displacement curves for Examples 4.4 to 4.7

5. APPLICATION

This chapter presents the analysis of an externally prestressed segmental bridge which has been designed for physical testing. The response of the bridge is computed by the nonlinear finite element method described in Chapters 2 to 4. The model bridge is a three-span, precast-segmental, box-girder structure with external prestressing and dry joints with multiple shear keys. Figures 5.1 to 5.3 give the details of the model bridge.

The dimensions in the longitudinal direction of the structure are given in Fig. 5.1. Figures 5.2a and 5.2b show the cross sections of the regular segments within the spans and of the special pier segments, respectively. Welded-wire fabric meshes placed at the top and bottom of each flange provide the longitudinal reinforcement for the segments, with some additional reinforcing bars placed as shown in the cross sections. The transverse and diaphragm reinforcement are not shown in the figures. The closure strips have the same cross section as the regular segments. The external tendon profile is shown in Fig. 5.3. Figure B.1 gives the geometry and prestressing forces of the tendons at transfer used in all the analysis cases of this chapter. Also, few bonded internal tendons are prestressed through the upper flange of the model bridge (not shown). However, for the purpose of illustrating the effects of external prestressing and dry joints, the bonded internal tendons are not considered in the analyses, except where mentioned for comparative purposes.

The prestressing forces used in the analyses are applied before losses due to elastic shortening have occurred. However, those used in actual structures are applied after elastic shortening. Also, losses of prestress due to creep and shrinkage of concrete, and relaxation of tendons are not accounted for. For the purpose of this report, a realistic set of initial forces, as the ones used, are satisfactory to illustrate the general behavior of externally prestressed segmental bridges.

Some of the implicit assumptions in the finite element analysis might deviate the results here from the actual behavior, especially close to ultimate loads. These assumptions are: (1) all passive reinforcement is adequately developed, (2) no slippage of tendons at deviation points, (3) no shear failure through joints, (4) diaphragms

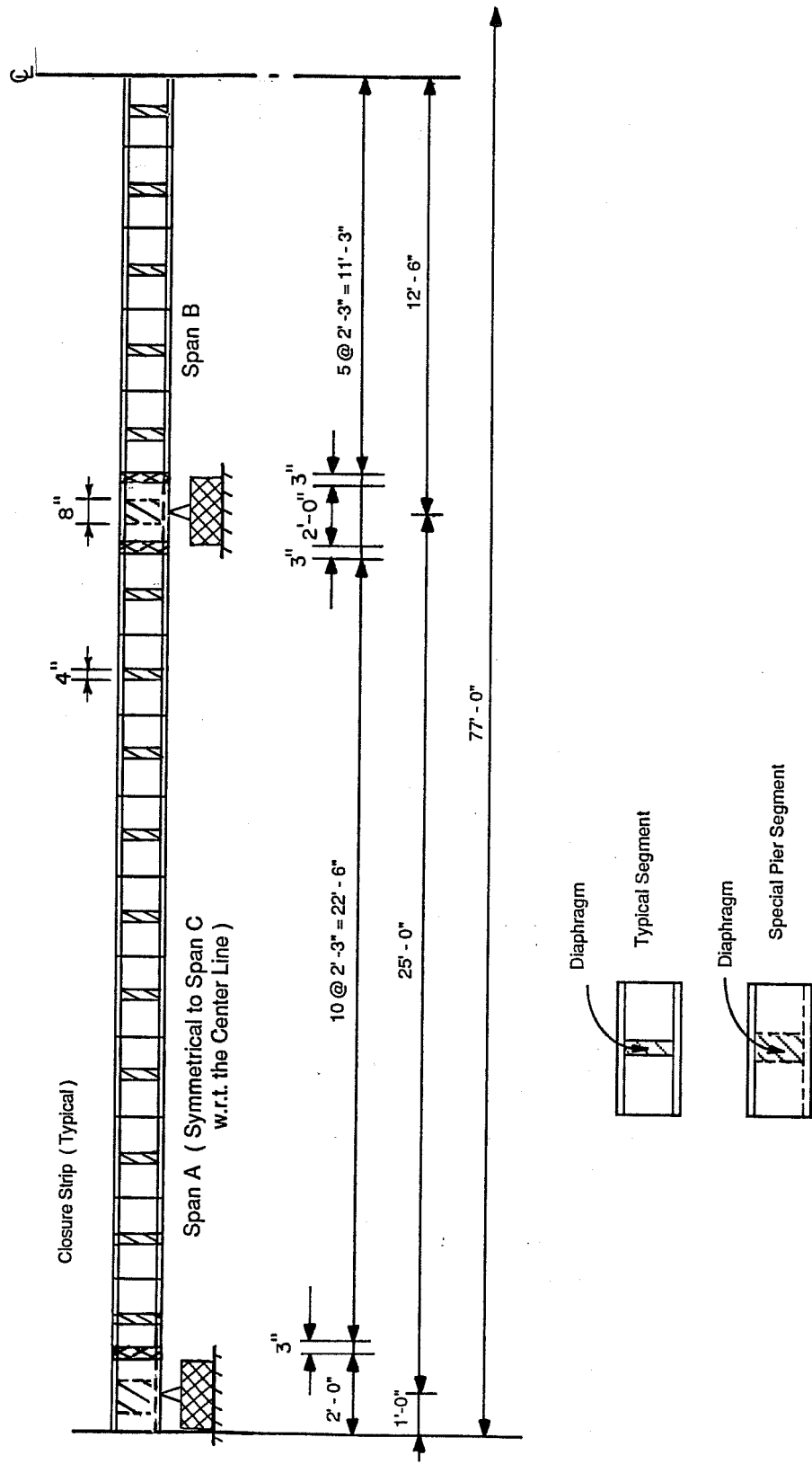


Fig. 5.1 Three span segmental bridge

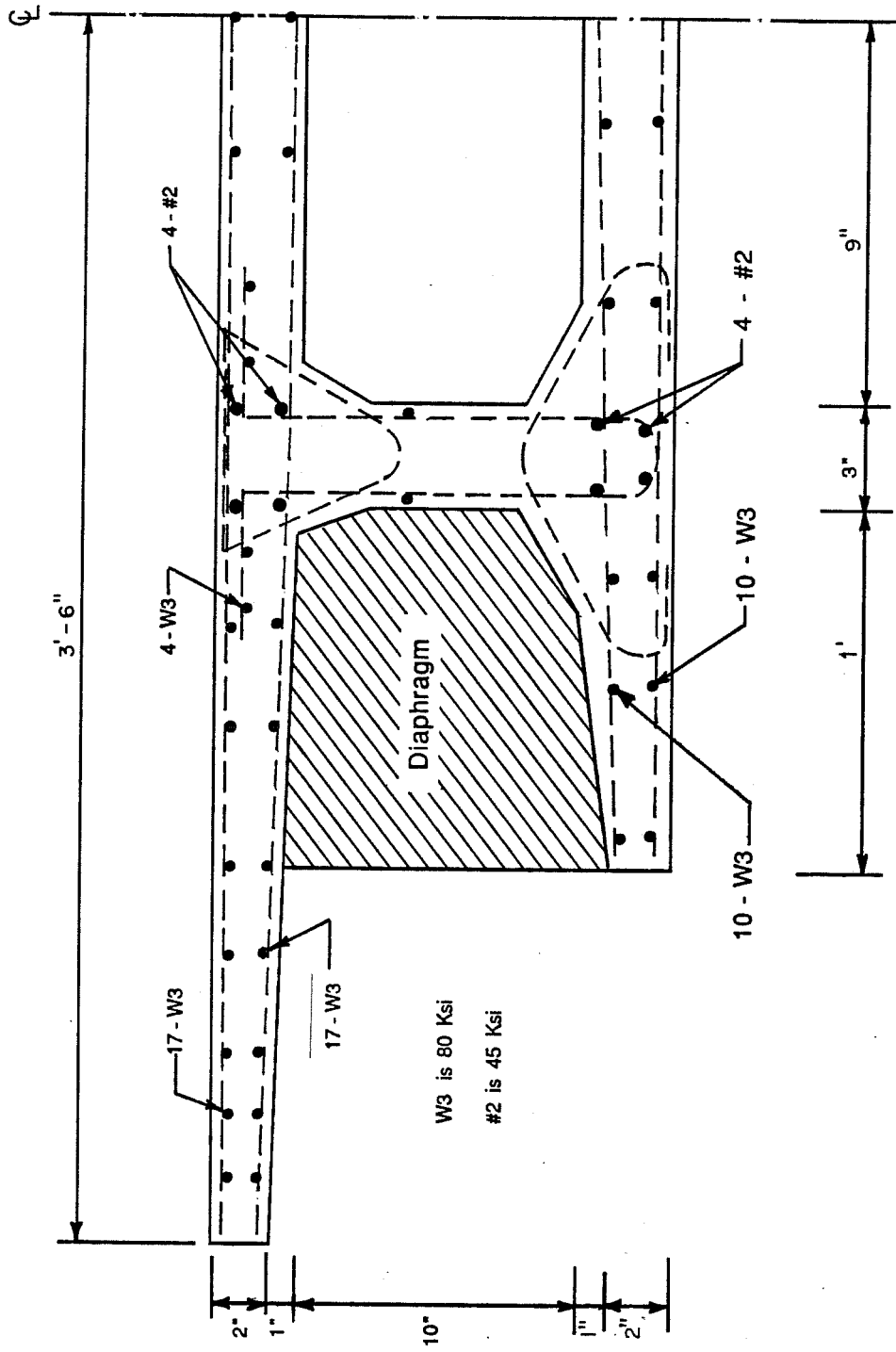


Fig. 5.2a Regular segment cross section

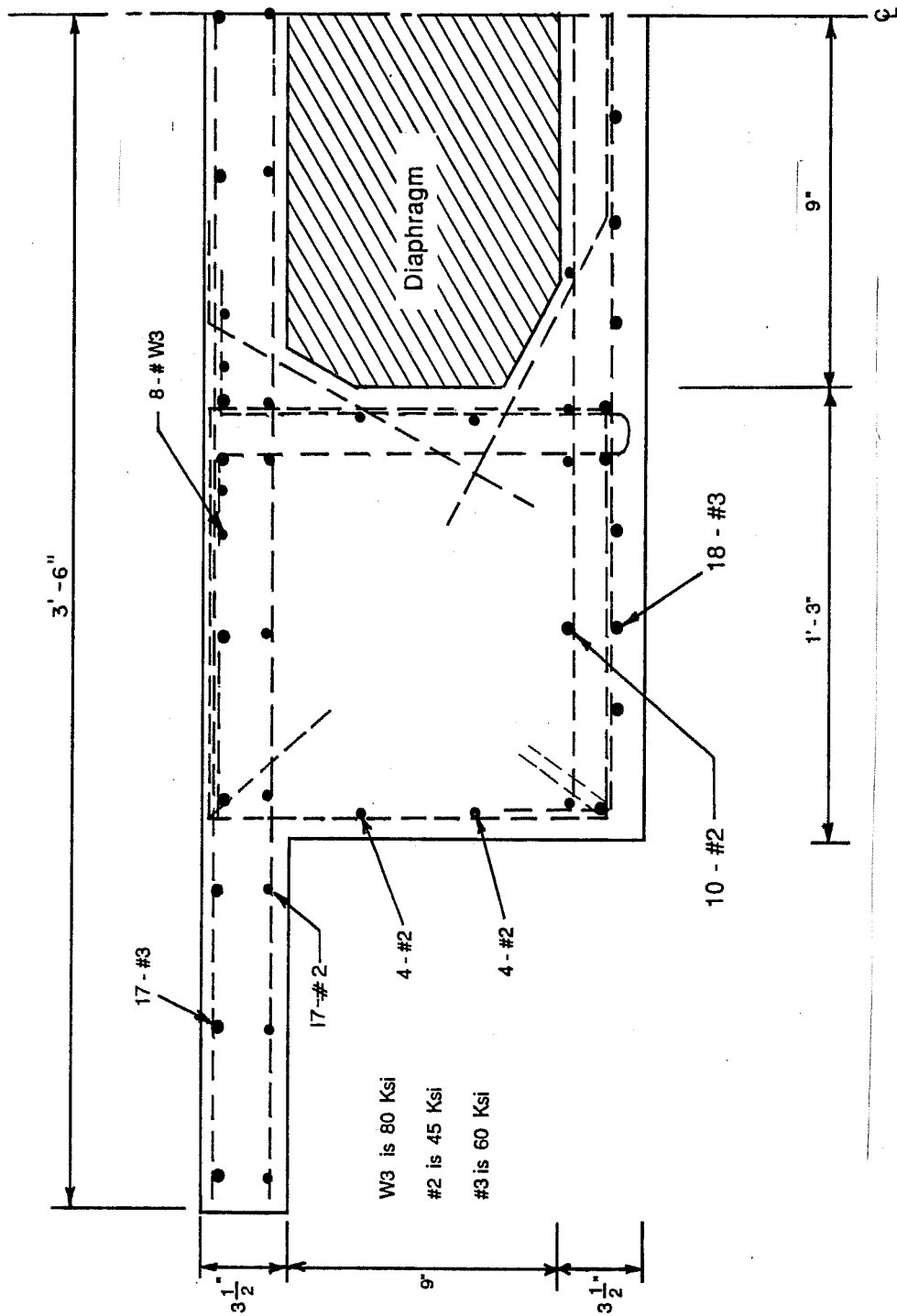


Fig. 5.2b Pier segment cross section

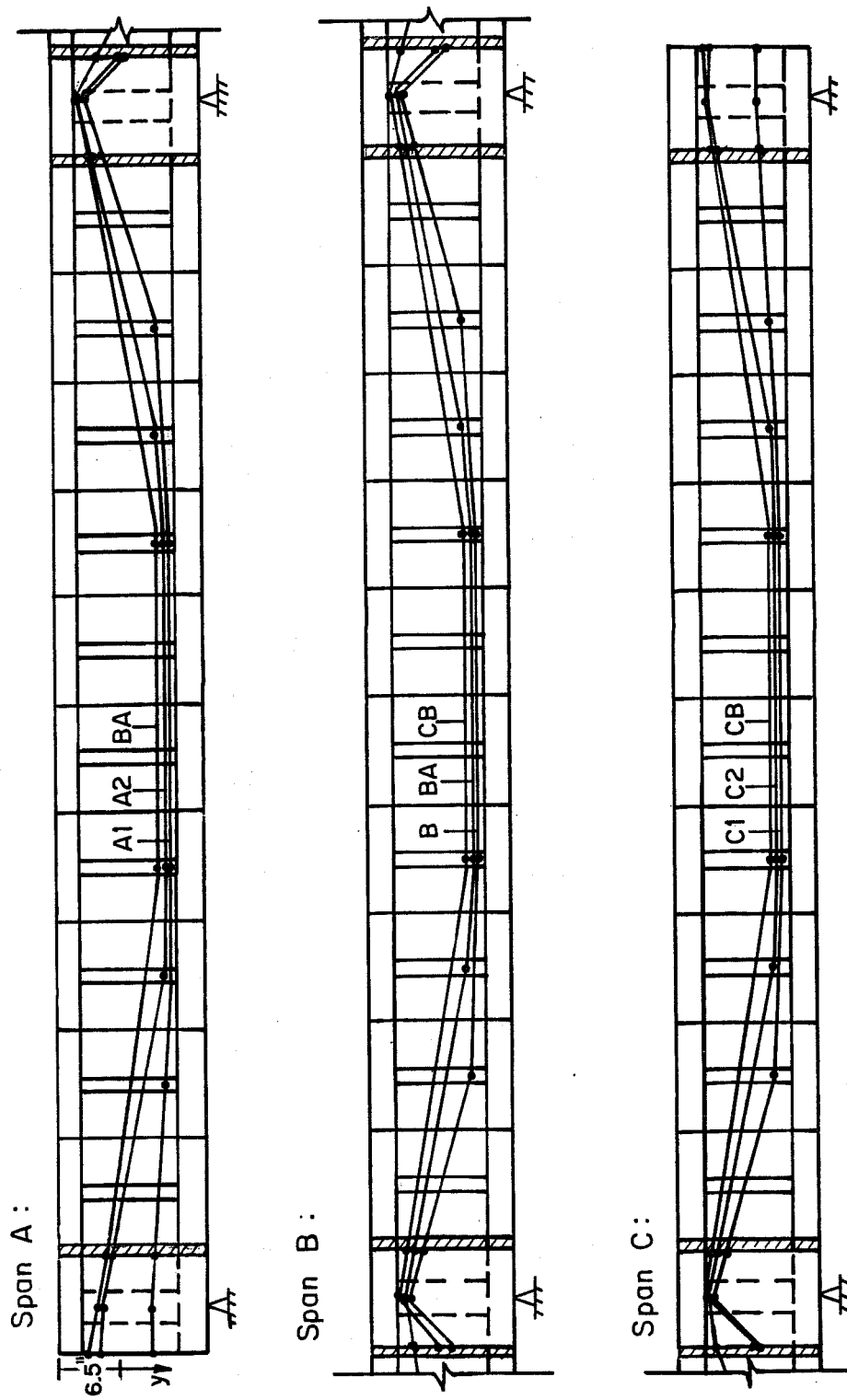


Fig. 5.3 External tendon profile for segmental bridge (geometry and stress are given in Fig. B.1)

are infinitely strong, and (5) the classical assumptions normally used for behavior of structures under service loads.

Since the formulation of the joint element assumes infinite strength, the finite element analysis resumes after the concrete reaches its nominal capacity at the critical joint. Termination conditions need to be separately determined for failure of joints. The linear gap-force relationship used in the element formulation is inappropriate for such calculations. An approximate method considering the nominal strength of the material is used as allowed by the ACI 318-83, Section 10.2.¹ The equilibrium at the joint is expressed, using ACI 318-83 notation, as:

$$f_{PS} A_{PS} = 0.85 f'_c \beta_1 cb$$

where $f_{ps} A_{ps}$ is the tensile force in the tendons, and $0.85 f'_c$ is an assumed uniformly distributed, concrete compression stress over a rectangular area of width b , and depth $\beta_1 c$, in the upper or lower flange. The results from the finite element analysis give another relationship between the total force of the tendons and the depth of contact, c . If both relationships are plotted, the intersection point determines when crushing occurs at the critical joint. The corresponding load is determined from the analysis.

The span-by-span construction procedure for externally prestressed bridges affects the state of stress in the bridge after erection, before application of live loads. For this model bridge, the sequence is to erect span A (Fig. 5.1) on shoring, prestress tendons A1 and A2 (Fig. 5.3), and remove shoring. Then, erect span B on shoring, prestress tendons B1 and BA, and remove shoring. Then, erect span C on shoring, prestress tendons C1, C2, and CB, and remove shoring. Finally, post-tension the top internal tendon and grout it. The deflected shape and stresses of the bridge are not the same as if the three spans were erected together on shoring, and then all the tendons were prestressed. Nevertheless, the bridge is analyzed here without taking into account its construction sequence. Linear analysis has shown that construction sequence has a small effect on service load stresses. The construction sequence, also, has no effect on the failure loads and mechanisms of the bridge.

In the finite element modeling, each segment is divided into two elements. The fiber models for the regular and pier segments are shown in Figs. 5.4a and 5.4b, respectively. The area of each fiber, the distance of their centroids from the reference

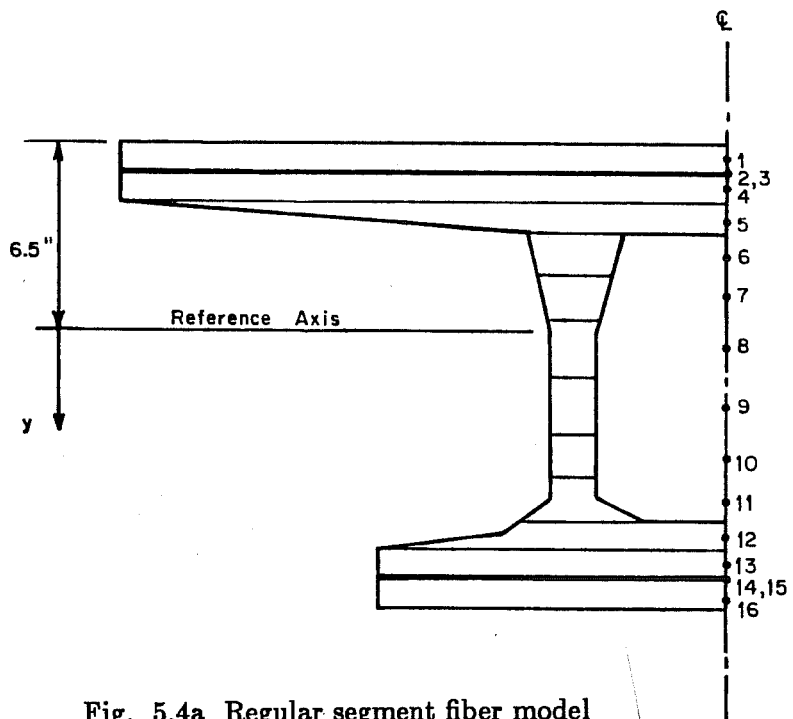


Fig. 5.4a Regular segment fiber model

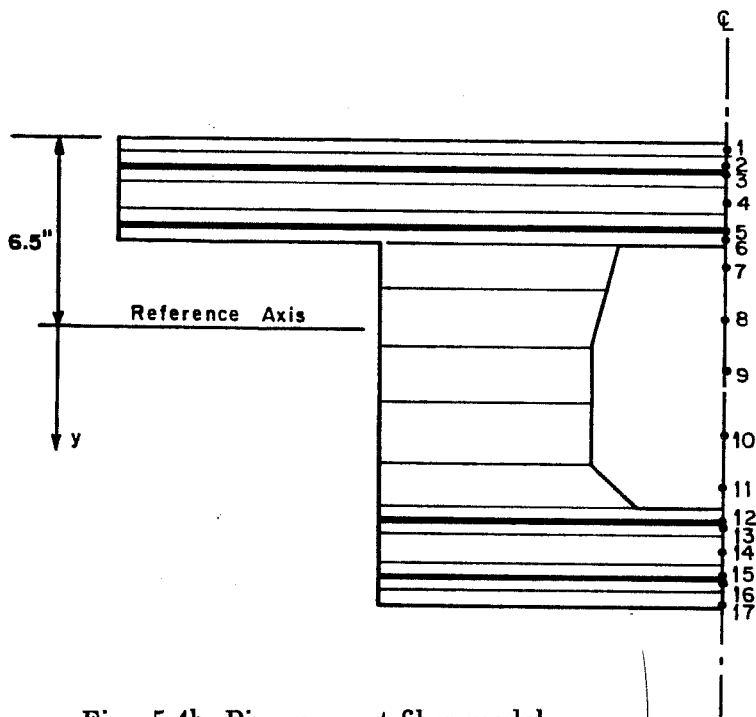


Fig. 5.4b Pier segment fiber model

axis, and material types are given in Tables 5.1a and 5.1b. The closure strips are considered as separate elements with the same cross section as the regular segments, but without reinforcement. The materials are idealized by a second-degree, nonlinear stress-strain curve for concrete (Fig. 5.5), and bilinear curves for the reinforcing steel (Fig. 5.6). Table 5.2 lists the properties of the material types in the segments. The external tendons are divided into elements that span between anchorage locations and deviation points at the diaphragms, with a bilinear stress-strain relationship (Fig. 5.7). Each joint, including both sides of the closure strips, is modeled as a joint element with a stiffness of $1. \times 10^5$ K/in./in.

The weight of the typical segments is 0.451 K/ft. Addition of concrete blocks to simulate actual behavior creates a total dead load of 1.804 K/ft. In all the analysis cases of this chapter, the dead loads are applied at the nodes using tributary areas, and are referred to as DL. The following examples consider the behavior of the model bridge for various live load cases.

Example 5.1: Segmental Versus Monolithic

In this example, the model bridge is compared to a similar monolithic bridge, where the reinforcement is assumed continuous except through the closure strips. Both structures are subjected to a concentrated live load at the interior midspan. The load is incremented up to failure which is manifested by either the crushing of concrete at a joint (segmental bridge only), or by the divergence of the computer solution due to other failure schemes. The segmental bridge fails when the interior midspan joint opens to about 94.4% and the concrete exceeds its compressive strength of 6 ksi at the joint. However, the monolithic bridge first forms a hinge at the center when the corresponding active and passive reinforcements yield. Then, a mechanism occurs when two other hinges form at the closure strips of the interior span because concrete reaches ultimate strength at the bottom fibers.

The live load versus displacement, joint percentage opening and width, and stress for one of the tendons at the interior midspan for both bridges are plotted in Figs. 5.8, 5.9, and 5.10. In the segmental bridge, the interior midspan joint opens under small load and it reaches 80% of the total depth at 25 K live load. However, the joint width remains negligible and tendon stresses experience small change. Beyond this force, the bridge becomes more flexible as the joint width increases noticeably

Table 5.1 Model for Regular and Pier Segments

Fiber	Area (in. ²)	y (in.)	Material*
1	84.0	-6.0	C
2	1.26	-5.5	S3
3	0.40	-5.5	S1
4	84.0	-5.0	C
5	54.0	-4.09	C
6	15.9	-2.78	C
7	11.7	-1.29	C
8	12.1	0.49	C
9	12.0	2.5	C
10	9.0	4.25	C
11	18.0	5.65	C
12	36.0	7.06	C
13	48.0	8.0	C
14	0.40	8.5	S1
15	0.60	8.5	S3
16	48.0	9.0	C

*See Figs. 5.5 and 5.6 and Table 5.2.

C: Concrete

S: Steel

(a) Regular Segments

Fiber	Area (in. ²)	y (in.)	Material*
1	42.0	-6.0	C
2	84.0	-5.5	C
3	1.99	-5.44	S2
4	84.0	-4.5	C
5	0.85	-4.12	S1
6	84.0	-3.5	C
7	48.5	-2.25	C
8	61.7	-0.5	C
9	60.0	1.5	C
10	60.0	3.5	C
11	49.5	5.27	C
12	48.0	6.5	C
13	0.5	6.62	S1
14	48.0	7.5	C
15	48.0	8.5	C
16	1.98	8.71	S3
17	24.0	9.25	C

*See Figs. 5.5 and 5.6 and Table 5.2.

C: Concrete

S: Steel

(b) Pier Segments

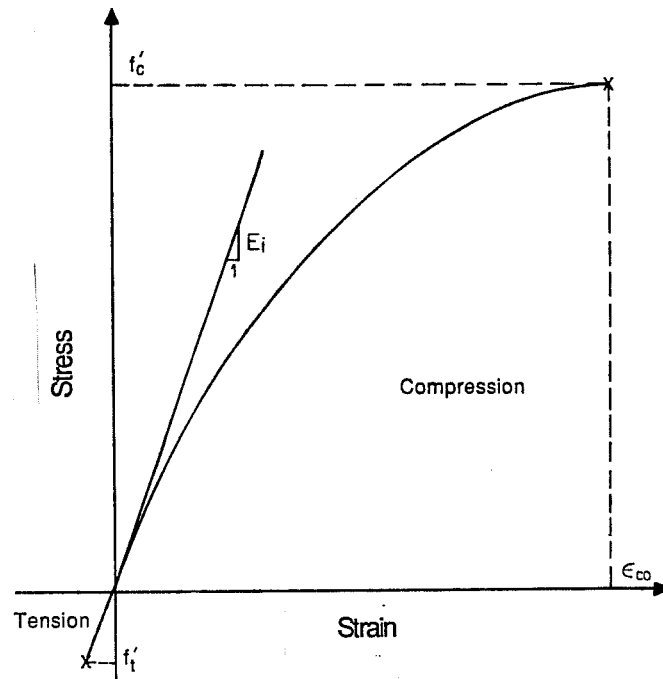


Fig. 5.5 Stress-strain relationship for concrete segments

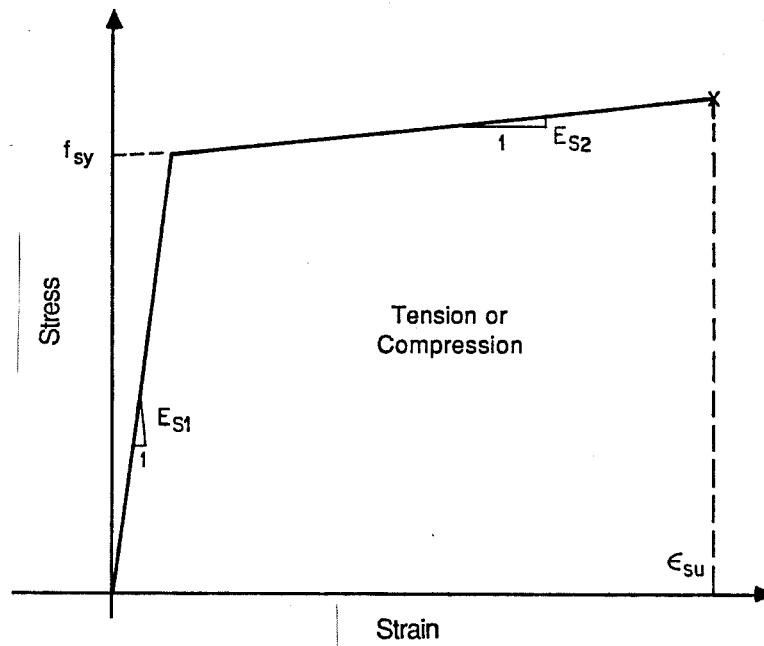


Fig. 5.6 Stress-strain relationship for reinforcing steel

Table 5.2 Material Properties for Concrete Segments and Reinforcing Steel

Material Type *	Description
C	$f'_c = 6.00$ Ksi $f'_t = 0.562$ Ksi $E_i = 5.50 \times 10^3$ Ksi $\epsilon_{co} = 2.20 \times 10^{-3}$
S1	$f_{sy} = 45.0$ Ksi $\epsilon_{su} = 0.16$ $E_{s1} = 29.0 \times 10^3$ Ksi $E_{s2} = 100$ Ksi
S2	$f_{sy} = 60.0$ Ksi $\epsilon_{su} = 0.21$ $E_{s1} = 29.0 \times 10^3$ Ksi $E_{s2} = 100$ Ksi
S3	$f_{sy} = 80.0$ Ksi $\epsilon_{su} = 0.28$ $E_{s1} = 29.0 \times 10^3$ Ksi $E_{s2} = 100$ Ksi

* See Table 5.1 and Figs. 5.5 and 5.6

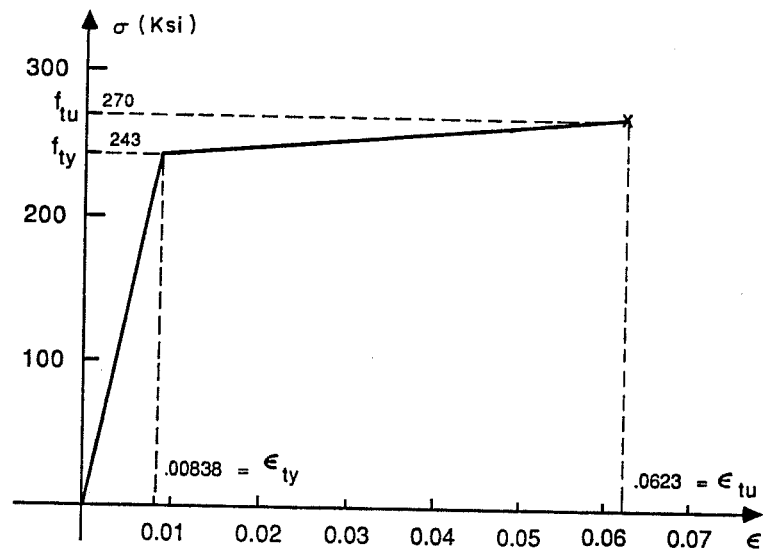


Fig. 5.7 Stress-strain relationship for external tendons

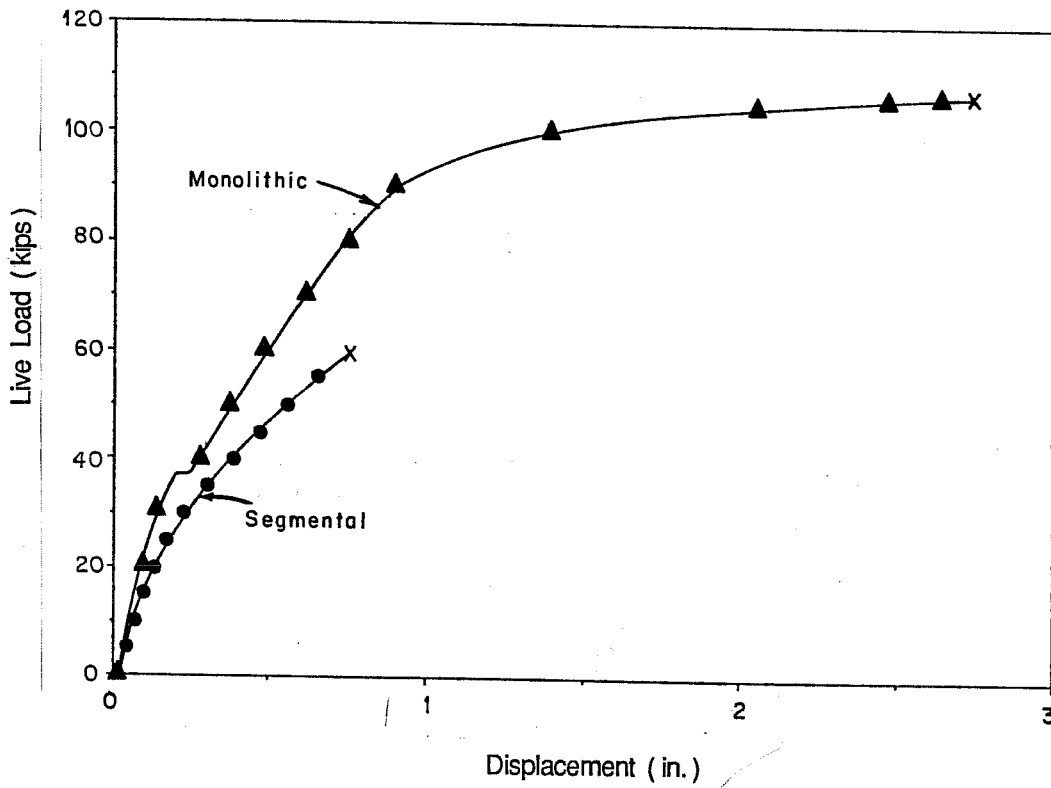


Fig. 5.8 Live load-displacement curve at interior midspan

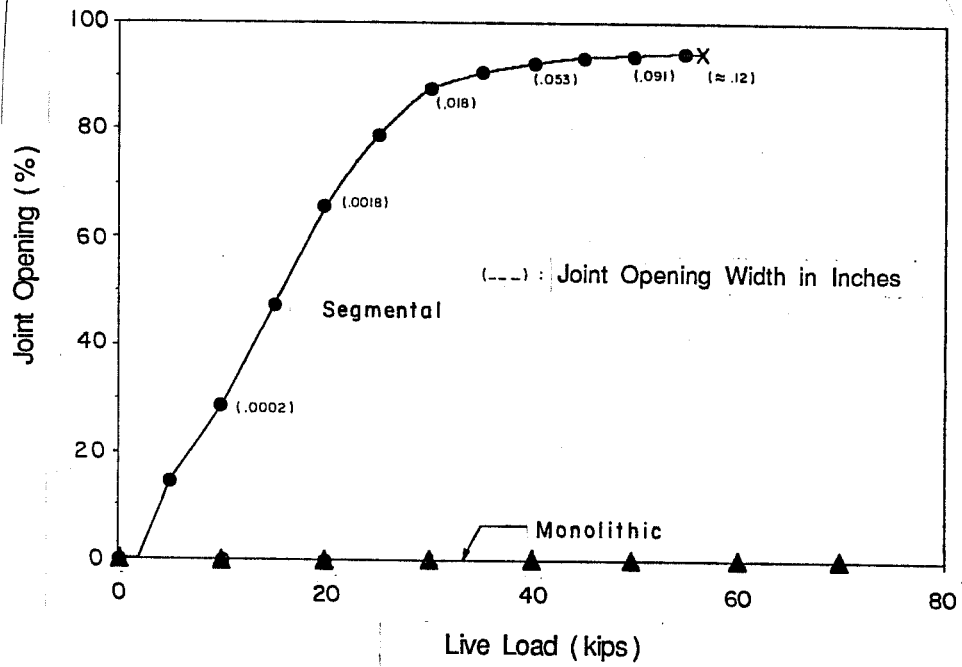


Fig. 5.9 Live load versus percentage opening of joint at interior midspan

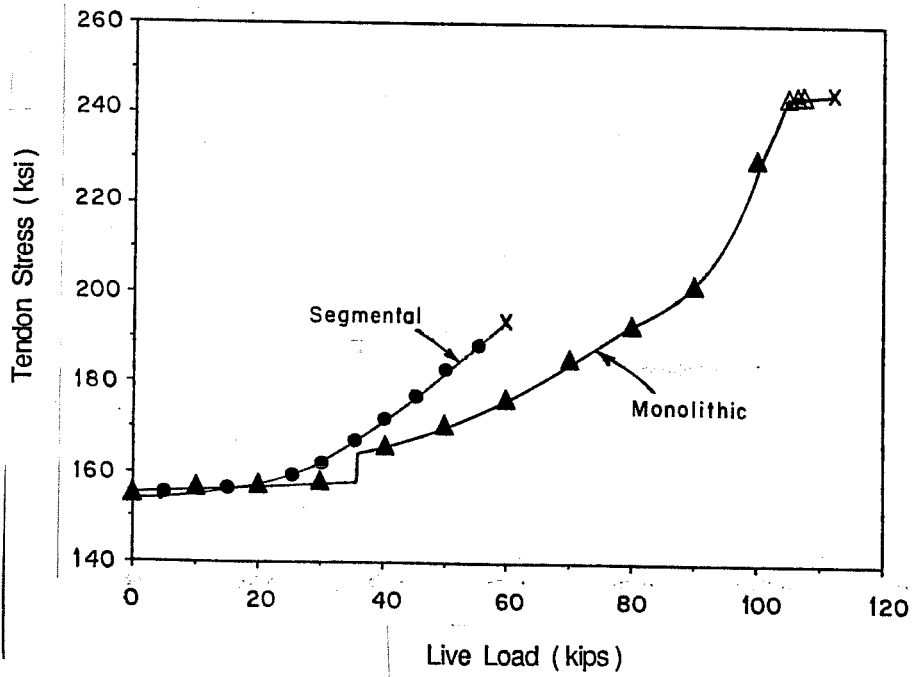


Fig. 5.10 Live load versus interior midspan stress of tendon B

and the tendons pick up larger tensile forces. The joints act as preset cracks, and the concrete segments do not experience any tensile cracking. This continues up to failure at about 56 K load and 0.67 in. displacement.

Explanations for the low strength and ductility of externally prestressed segmental bridges can be attributed to the existence of unbonded tendons and dry joints. Since the tendons between deviation points are free, the strain in the tendon is constant along its length, and the strain at the critical section is less than what it would be for internally bonded tendons under similar conditions. Hence, the stress in the tendons is increased only slowly, so that when the crushing strain has been reached in the concrete, stress in the steel is far below its ultimate strength (Fig. 5.10). Also, the existence of joints tend to concentrate the stresses in the concrete at the joints, thus resulting in early failure.

The main sources of error in this analysis near ultimate are the joint assumption that plane sections remain plane, and the estimated value of the stiffness per unit depth, k . When the joint width becomes large, the joint section cannot be considered plane anymore. Also, at a larger value of k , the percentage of joint opening is larger for the same load, which results in earlier failure.

In contrast, the monolithic bridge cracks in tension near the interior midspan when the load is about 37 K. As expected, a few large cracks appear in the middle instead of many small, well distributed ones. The interior midspan tendons yield at about 100 K and failure occurs at 108 K live load and 2.8 in. displacement. The absence of the joints eliminates the problem of concentrated stresses because the cracks are not as deep as the joint openings in the segmental bridge. Also, the presence of a large compression zone with high concrete strength allows the stress in the tendons to increase enough to develop yielding.

Example 5.2: Segmental Bridge With Bonded Internal Tendons

The segmental model bridge is considered here with bonded internal tendons in the top flanges of the segments. These tendons have the same material as the external tendons with a total cross-sectional area of 0.68 sq in. located at about 1.3 in. from the top with a prestressing force at transfer of 189 K (before elastic shortening). In the analysis the internal tendon is approximated by end forces, which are applied

at the reference axis of the elements, and an additional steel fiber in each segment. This approximation does not consider the effect of the variation of the internal tendon stresses through the joints. The results of this analysis are compared to those of the segmental bridge of Example 5.1. The capacity of the model bridge increases from 56 K to 65 K because of the internal tendons, where the failure mechanism remains the same. Also, the presence of the internal tendons increases the stiffness of the model bridge as expected. For the same load, the bridge with the bonded internal tendons has smaller deflection at the interior midspan (Fig. 5.11), less joint opening and smaller joint width (Fig. 5.12), and the stresses in the external tendons are smaller (Fig. 5.13).

Example 5.3: Segmental Model Bridge Subject to Service and Factored Live Loads

This example considers service and ultimate load cases that cause critical conditions in the segmental model bridge. For the service loads, tributary values of scaled truck loadings are applied at the nodes, Fig. 5.14. These service loads, SL1 and SL2, are multiplied by an increasing load factor, LF, that increments by 0.5 until failure. Critical joint openings and joint widths, tendon stresses, and concrete fiber stresses are plotted and analyzed.

$DL + LF \times LS1$ causes maximum moment at the exterior midspan A. However, due to the non-symmetric tendon stresses and the use of tributary live loads, either the A or C midspan may control. At service loads ($LF = 1.0$), all the joints remain closed. As load increases, more and more joints open from the bottom side of spans A and C, and the top side of span B. Joint percentage openings and widths for load factors of 4.0 and 6.5 are given in Fig. 5.15. The compressive force between two consecutive deviators is constant, so concrete maximum stress in that zone occurs at the joint with the largest percentage opening. Figure 5.15 also identifies all the deviators and the critical locations. For three of the critical joints, the percentage opening, width, and one corresponding tendon stress versus the load factor are plotted in Figs. 5.16, and 5.17. The widths of the joints and the change in tendon stresses remain very small up to a load factor of 5.0. Beyond this load, the increase in joint widths and tendon stresses is more noticeable. Maximum tensile and compressive concrete stresses occur in the segments neighboring critical joints. Top

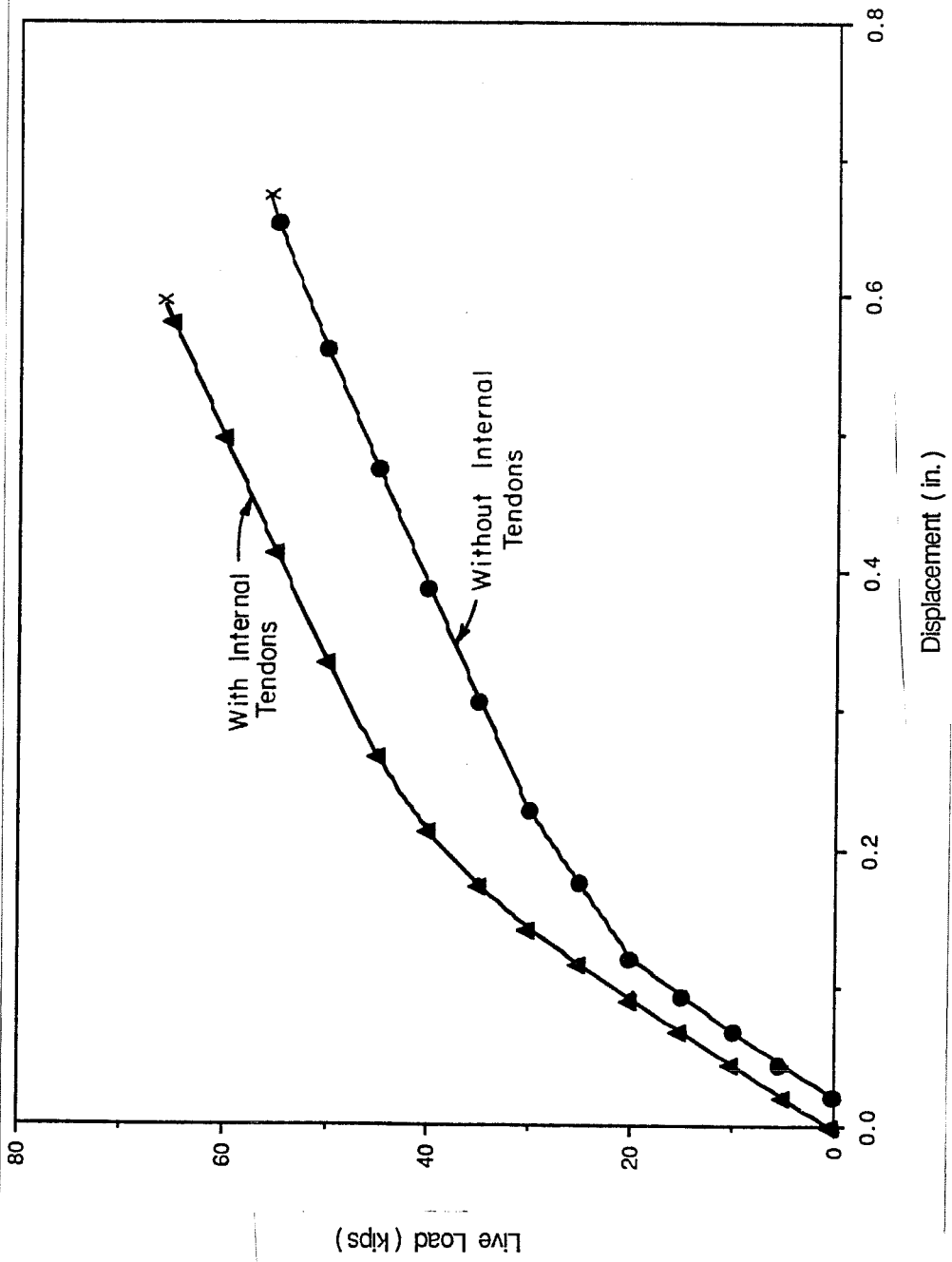


Fig. 5.11 Live load-displacement curves at interior midspan

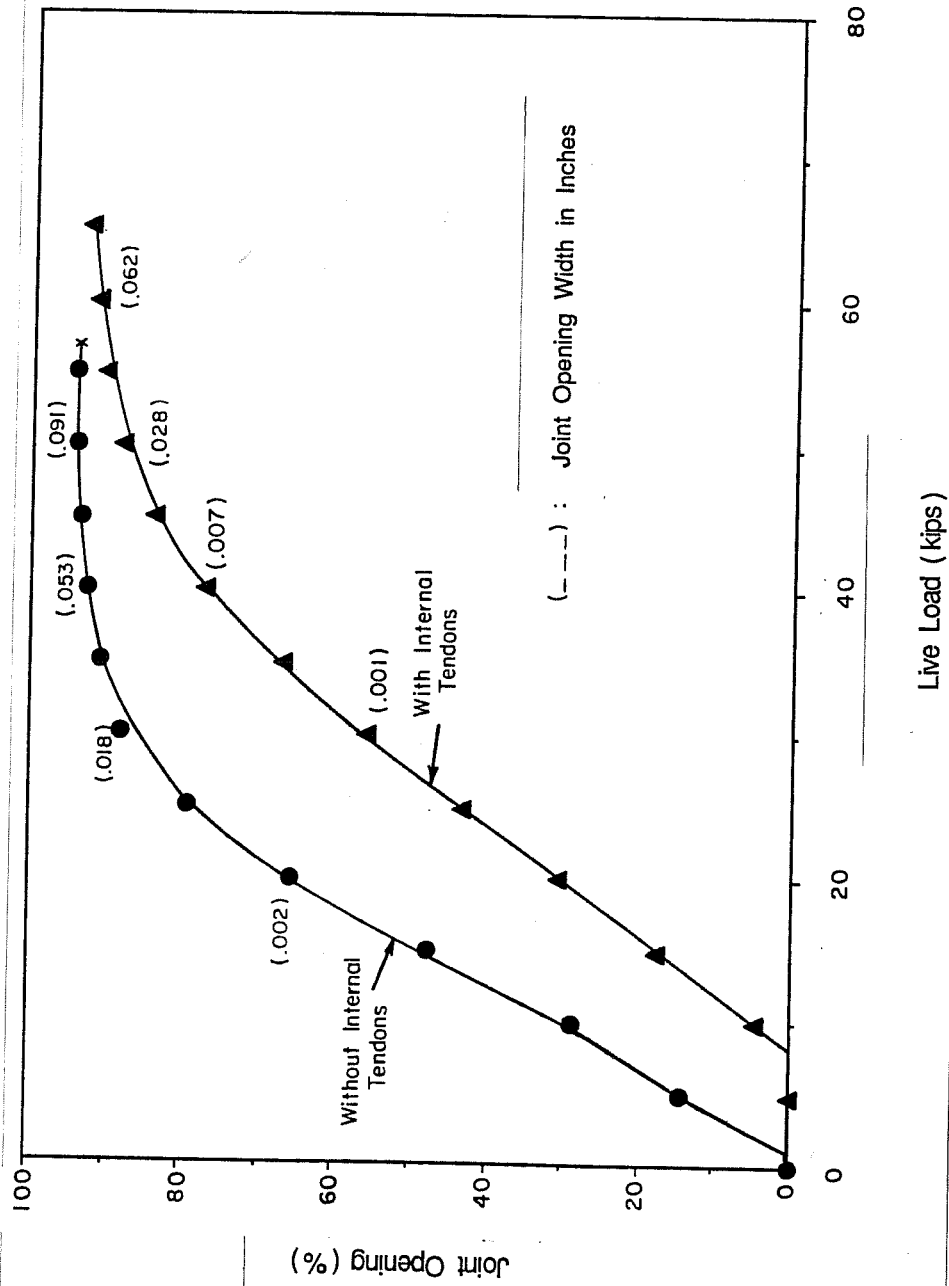


Fig. 5.12 Live load versus joint percentage opening at interior midspan

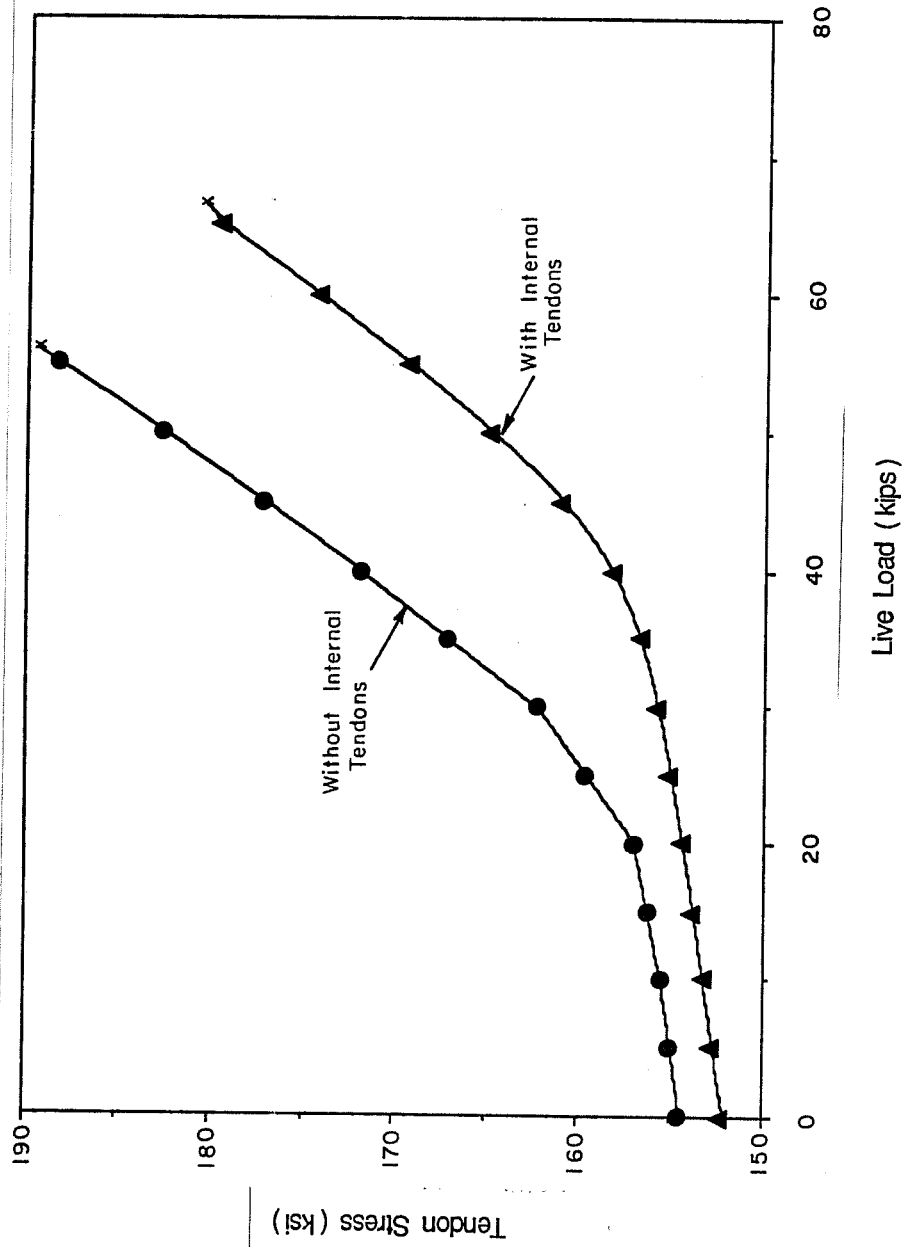
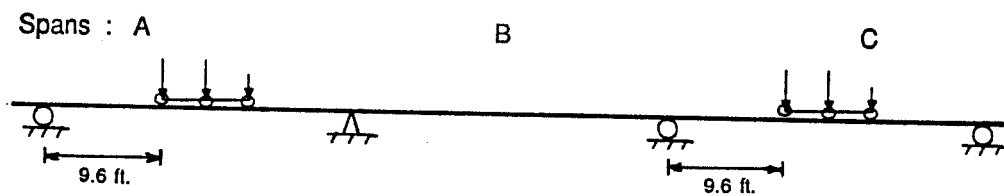
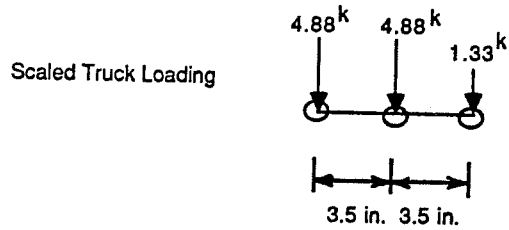
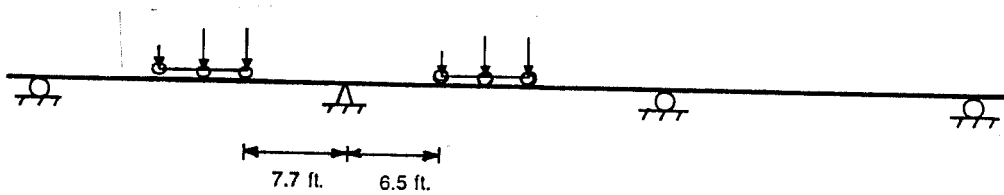


Fig. 5.13 Live load versus interior midspan stress of tendon B



(a) LS1



(b) LS2

Fig. 5.14 Service live loads

LF = 6.5		LF = 4.0		Joint Number
Joint Opening * (%)	Joint Width (in.)	Joint Opening * (%)	Joint Width (in.)	
0	0	0	0	1
0	0	0	0	2
23.34	.0002	0.09	~ 0	3
51.46	.0010	15.95	.0001	4
82.79	.0130	38.28	.0005	5
90.06	.0490	62.28	.0020	6
91.01	.0610	64.84	.0024	7
59.65	.0020	42.03	.0006	8
49.45	.0009	18.16	.0001	9
0	0	0	0	10
0	0	0	0	11
0	0	0	0	12
0	0	0	0	13
-46.65	.0005	0	0	14
-48.52	.0005	0	0	15
-72.29	.0026	0	0	16
-85.02	.0110	-5.01	~ 0	17
-83.41	.0084	-2.09	~ 0	18
-77.01	.0040	0	0	19
-72.77	.0027	0	0	20

* Bottom joint opening is positive

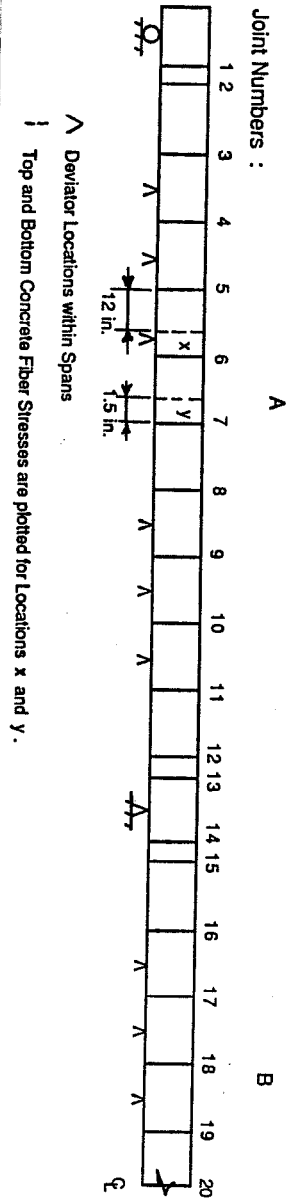


Fig. 5.15 Joint percentage openings and widths for load factors 4.0 and 6.5 of LS1 for all joints

(to be continued)

LF = 6.5		LF = 4.0		Joint Number
Joint Opening * (%)	Joint Width (in.)	Joint Opening * (%)	Joint Width (in.)	
-72.77	.0027	0	0	20
-77.80	.0044	0	0	21
-83.35	.0086	-3.82	0	22
-87.07	.015	-6.97	0	23
-71.56	.0026	0	0	24
-45.36	.0004	0	0	25
-43.18	.0004	0	0	26
0	0	0	0	27
0	0	0	0	28
0	0	0	0	29
10.21	.0001	0	0	30
66.01	.0024	28.60	.0002	31
75.62	.0066	54.21	.0011	32
92.93	.0970	66.83	.0027	33
76.78	.0075	53.06	.0011	34
74.14	.0052	29.70	.0003	35
42.72	.0006	9.60	.0001	36
17.02	.0001	0	0	37
0	0	0	0	38
0	0	0	0	39

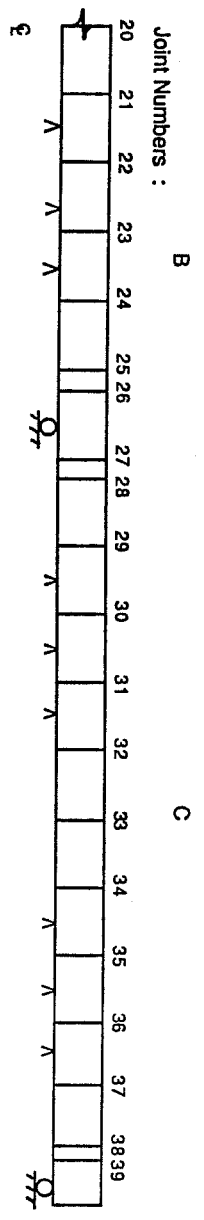


Fig. 5.15 (continued)

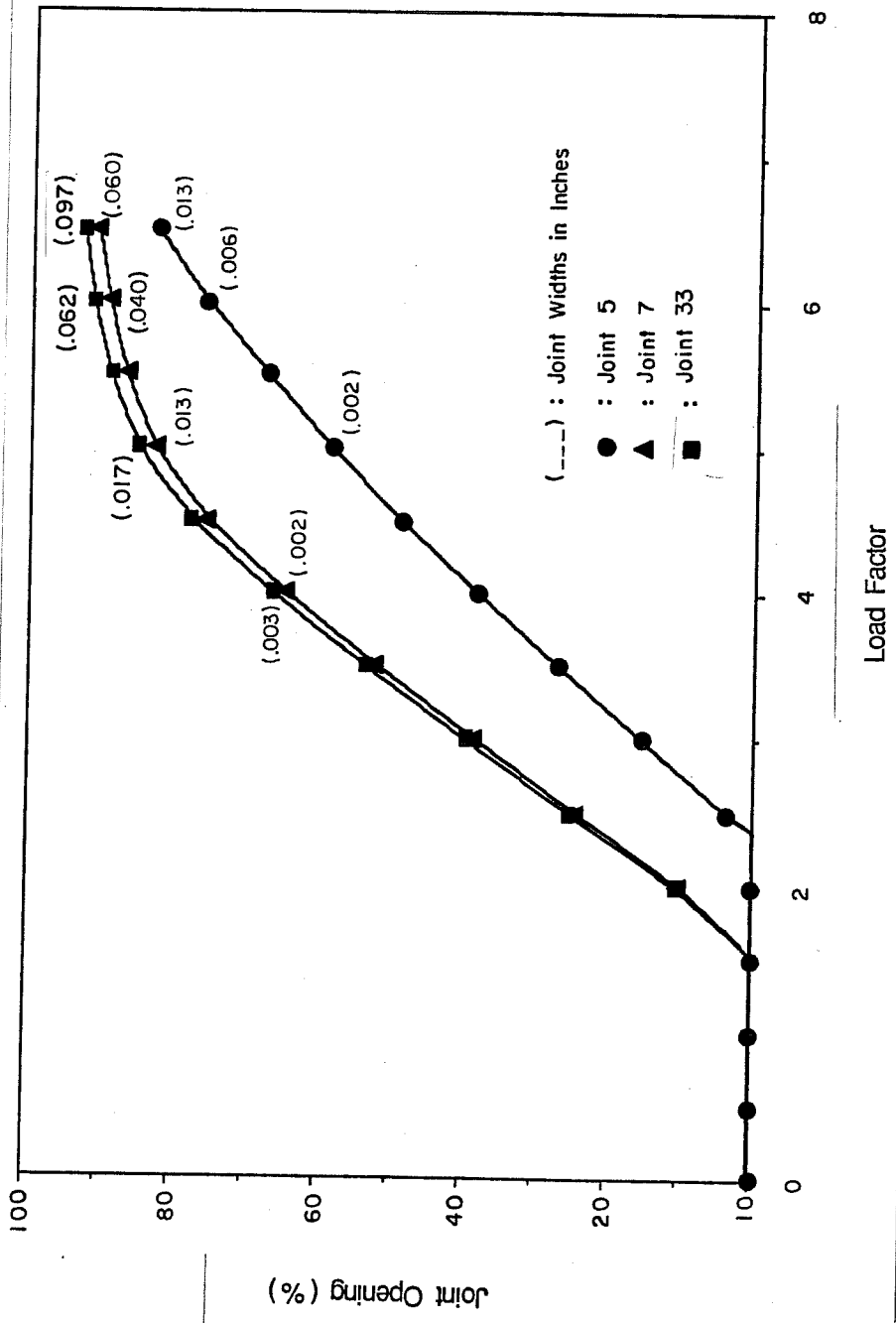


Fig. 5.16 Load factor for LS1 versus percentage opening of specified joints

and bottom fiber stresses at two locations are plotted in Fig. 5.18. Failure occurs when concrete at midspan C crushes in compression, at about $LF = 6.5$, just before midspan A could fail.

$DL + LF \times LS2$ causes maximum negative moment at the left interior support. Figure 5.19 identifies critical locations and lists joint percentage openings and widths for load factors of 4.5 and 6.0. Joint percentage openings and widths at A and B midspans and the interior support in between are plotted versus LF in Fig. 5.20. For each joint, the stress of one corresponding tendon is given in Fig. 5.21. Also, Fig. 5.22 shows top and bottom fiber stresses in the pier segment and neighboring regular segment around the critical joint. Beyond the load factor of 4.0, the widths of critical joints become noticeable and continue to increase up to failure. The interior closure strip at the support between spans A and B crushes at about the load factor of 6.0.

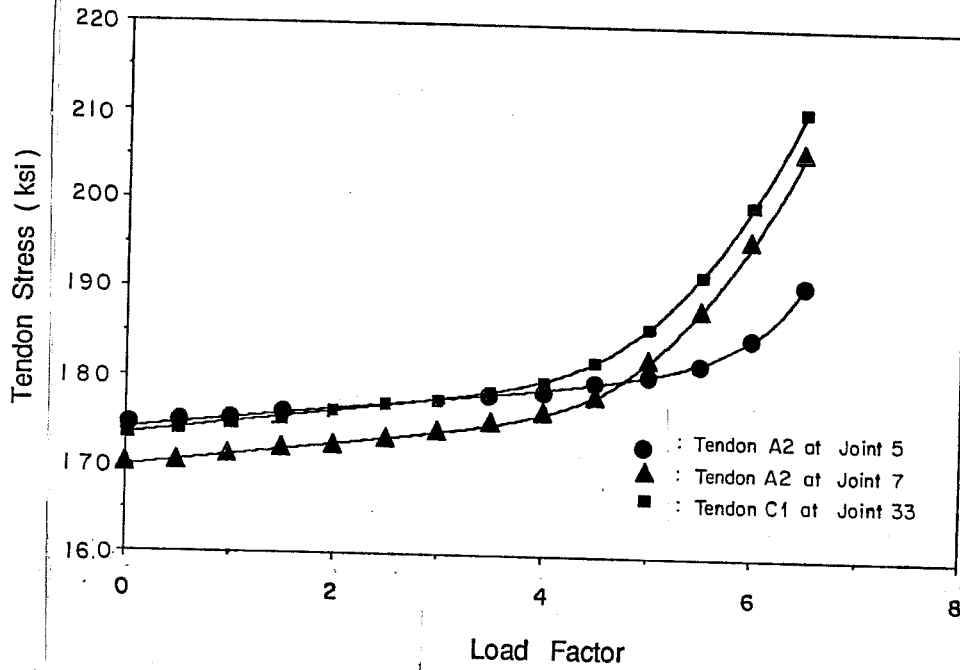


Fig. 5.17 Load factor of LS1 versus stresses of specified tendons at critical joints

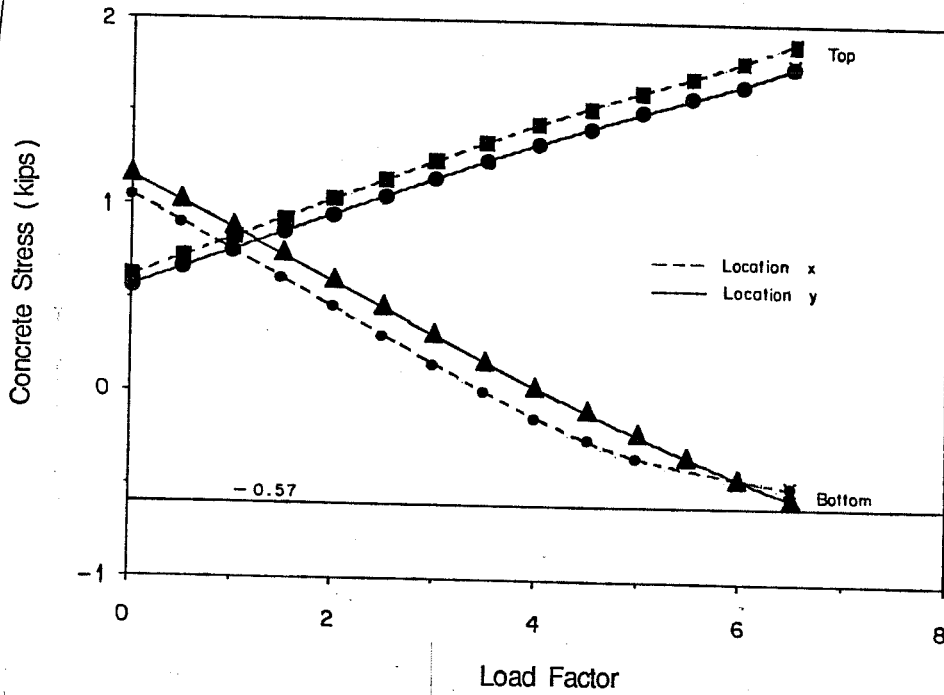


Fig. 5.18 Load factor of LS1 versus top and bottom concrete fiber stresses at specified locations (See Fig. 5.15.)

LF = 6.0		LF = 4.5		Joint Number
Joint Opening * (%)	Joint Width (in.)	Joint Opening * (%)	Joint Width (in.)	
0	0	0	0	1
0	0	0	0	2
0	0	0	0	3
4.11	~0	0	0	4
21.93	.0002	0	0	5
48.79	.0008	19.00	.0001	6
62.48	.0020	28.92	.0003	7
52.70	.0011	19.51	.0001	8
27.66	.0002	0	0	9
0	0	0	0	10
0	0	0	0	11
-23.29	.0002	-5.15	~0	12
-28.62	.0002	-8.59	~0	13
-90.75	.0320	-71.18	.0024	14
-83.14	.0088	-64.47	.0014	15
-21.07	.0001	-11.07	~0	16
0	0	0	0	17
38.04	.0003	1.97	.0001	18
80.36	.0070	69.64	.0023	19
92.73	.0590	85.29	.0120	20

* Bottom joint opening is positive

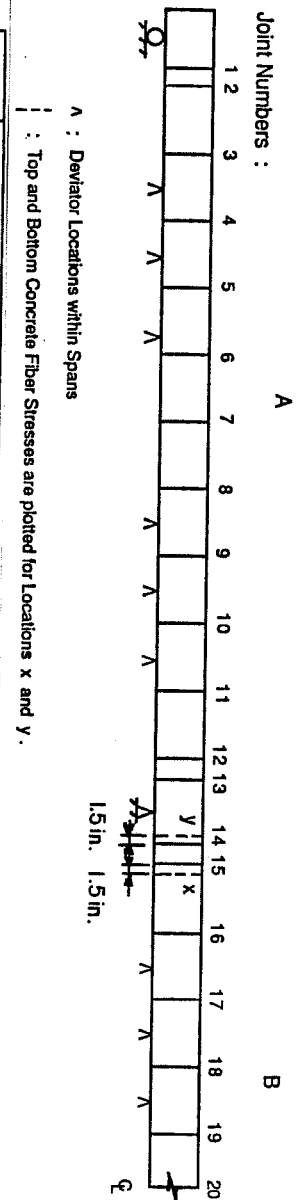


Fig. 5.19 Joint percentage openings and widths for load factors 4.5 and 6.0 of LS2 for all joints

(to be continued)

LF = 6.0		LF = 4.5		Joint Number
Joint Opening * (%)	Joint Width (in.)	Joint Opening * (%)	Joint Width (in.)	
92.73	.0590	85.29	0.12	20
66.59	.0020	67.19	.0020	21
33.85	.0002	33.12	.0002	22
0	0	0	0	23
0	0	0	0	24
0	0	0	0	25
0	0	0	0	26
0	0	0	0	27
0	0	0	0	28
0	0	0	0	29
-14.68	.0001	0	0	30
-12.10	.0001	0	0	31
-1.58	0	0	0	32
0	0	0	0	33
0	0	0	0	34
0	0	0	0	35
0	0	0	0	36
0	0	0	0	37
0	0	0	0	38
0	0	0	0	39

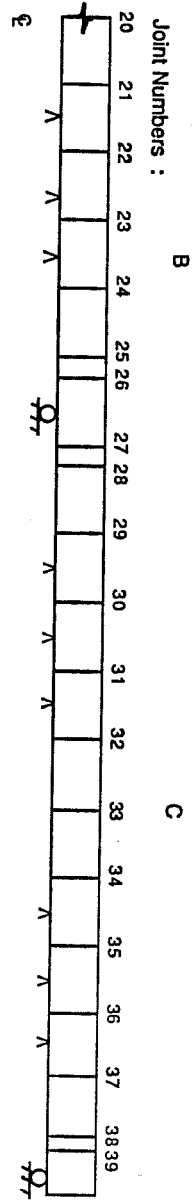


Fig. 5.19 (continued)

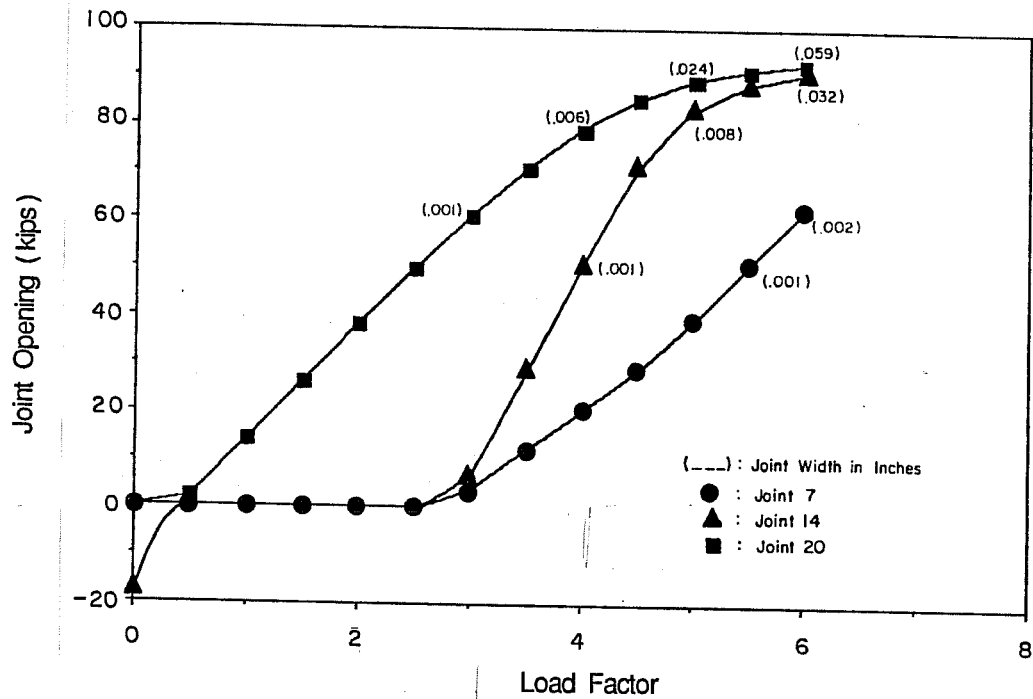


Fig. 5.20 Load factor of LS2 versus percentage openings of specified joints

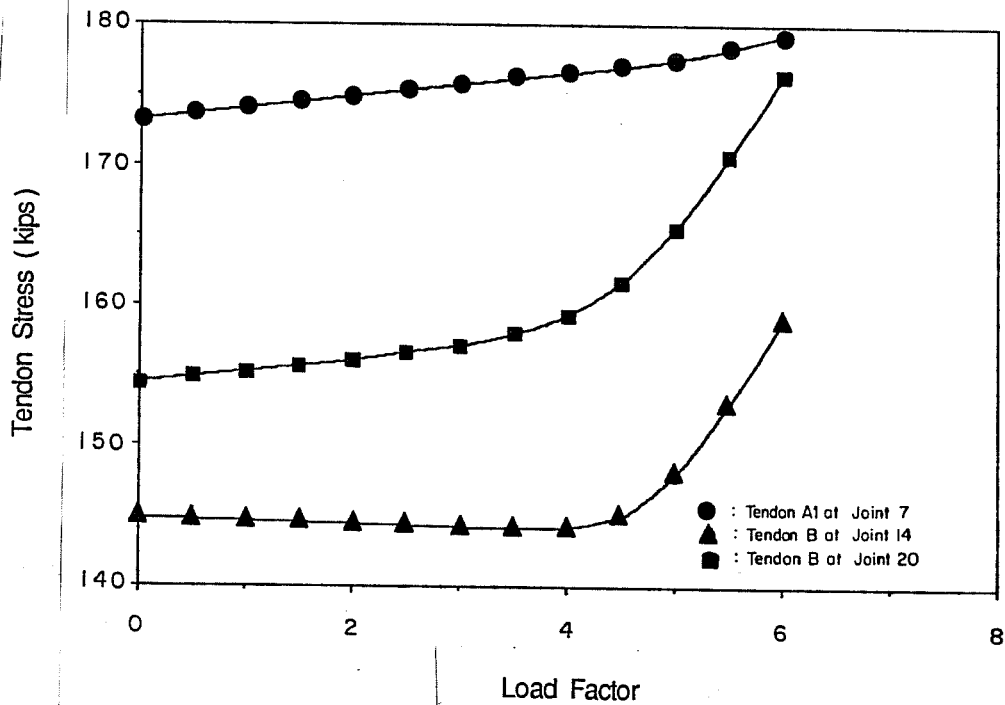


Fig. 5.21 Load factor of LS2 versus stresses of specified tendons at critical joints

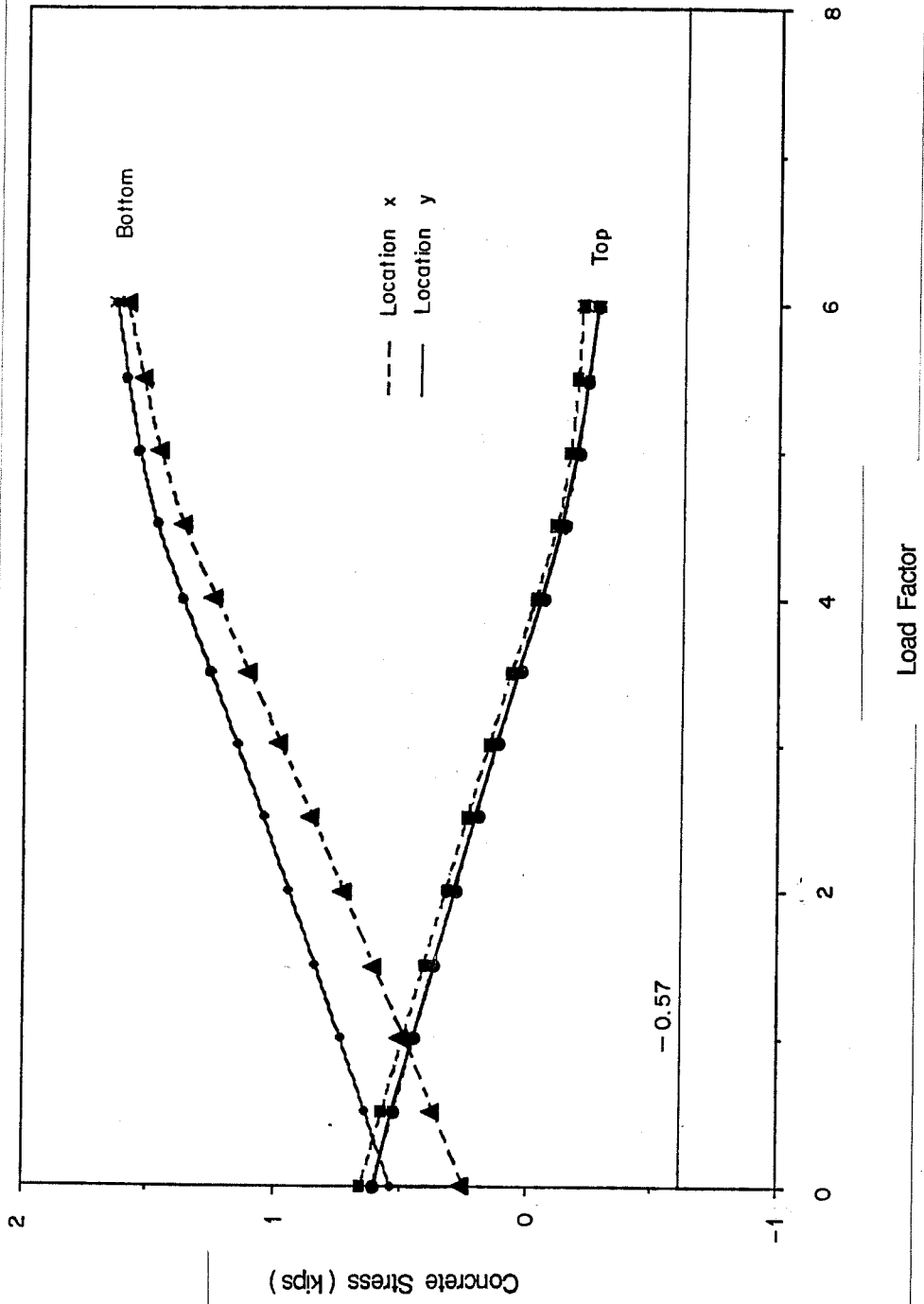


Fig. 5.22 Load factor of LS2 versus top and bottom concrete fiber stresses at specified locations (See Fig. 5.19.)

6. SUMMARY AND CONCLUSIONS

In this report, a finite element formulation for modeling externally prestressed segmental bridges has been developed using beam, external tendon, and joint elements. A nonlinear solution procedure for the equilibrium equations has been used to compute the response of bridges under static loads. The solution procedure is implemented in a computer program to perform analyses. The adequacy of the theory is verified with simple examples, and the effects of the joints and external tendons are examined. The sensitivity of the calculations due to the important parameters in the model are assessed. A bridge model designed for physical testing is presented, and its response to various load levels is computed. The examples use critical loadings to study the behavior of the bridge.

The finite element analysis presented gives realistic results when externally prestressed segmental bridges are adequately modeled. Increasing the number of fibers away from the neutral axis in a cross section, especially for nonlinear ranges of the materials, improves the results. Also, in the regions where axial strain is not constant and curvature is not linear, increasing the number of elements decreases the errors compared to known solutions. The materials need to be well modeled to predict actual behavior. To avoid divergence and errors due to solution methods, small load increments should be used.

The results show that externally prestressed segmental bridges are not as strong and ductile as bridges without joints or bridges with internal tendons. Large transfer tendon forces are needed to avoid joint openings under service loads. These forces also increase the strength by delaying large openings of critical joints. If ductility of the bridges is to be increased, the transfer stresses should be increased to values closer to the yield stress of the tendons.

APPENDIX A

USER INSTRUCTIONS FOR COMPUTER PROGRAM

Introduction

The computer program developed to carry out analysis for the finite element theory presented in this report is written in FORTRAN IV . Program FEAP⁶ (by R. L. TAYLOR, Department of Civil Engineering, University of California, Berkeley, California 94720, U.S.A.) is used as a basis in developing the program. The program has the ability to be extended to handle general finite element problems, and hence some of the variables defined may not be applicable to the specific applications here. The instructions will refer particularly to segmental bridges with external tendons. The size of the problem is controlled by the dimension of blank COMMON and the value of MAX as set in the main program. All arrays must reside in the central memory.

Modeling

The solution of a finite element problem using this program begins with a sketch of a mesh covering the bridge to be analyzed including beam, tendon, and joint elements only. All the nodes are located along a chosen reference axis throughout the bridge.

The next step is to number the elements and nodes in consecutive order. The beam elements are numbered first, followed by the tendon and joint elements, where the order of numbering within any type of elements is not crucial. However, the order of numbering the nodes influences the efficiency of the solution, and the best way is from one side of the bridge to the other. Two consecutive node numbers are assigned at the joint with the same coordinates.

Input Data

Once the sketch and numbering of the mesh is completed the user can prepare the input data for the program. The first step consists of specifying problem title and control information given in Table A.1, which is used during subsequent data input and to allocate memory in the program.

Table A.1 Title and Control Information Formats

Title Card-FORMAT (20A4)

Columns	Description
1 to 4	Must contain FEAP
5 to 80	Alphanumeric information to be printed with output as page header

Control Card-FORMAT (16I5)

Columns	Description
1 to 5	Number of nodes
6 to 10	Number of elements
11 to 15	Number of material sets
16 to 20	Spatial dimension (≤ 3)
21 to 25	Number of unknowns per node (3)
26 to 30	Number of nodes per element (2)
31 to 35	Added size to element matrices (0)
36 to 40	Number of nodes subject to increment loading
41 to 45	Maximum number of fibers (≤ 25)
46 to 50	Number of different fiber sets
51 to 55	Number of elements with fibers

Once the control data is supplied, the program expects the data cards for the mesh description such as nodal coordinates, element connections, etc. The flow of data to the program is controlled by a set of macro commands. The available commands are given in Table A.2. PRIN, and NOPR macro commands allow the user to print and suppress printing, respectively, of any data which is input subsequently. Thus, once a mesh has been fully checked it is not necessary to reprint all the mesh data.

An analysis will require:

- (a) coordinate data which follows the macro command COOR and is prepared as described in Table A.3;
- (b) element data which follows the macro command ELEM and is prepared according to Table A.4;
- (c) material data which follows the macro command MATE and is prepared according to Table A.5 including data required for each particular element; and
- (d) boundary restraint conditions and joint specification which follow the macro command BOUN and is prepared according to Table A.6.

In addition, most analyses require specification of nodal force or displacement value, macro FORC, which is specified according to Table A.7. The end of any mesh data is indicated by use of an END macro card.

As an example of the data input required to describe a mesh consider Fig. A.1 as a segmental bridge with external tendons. The input data for this problem are shown in Table A.8.

At the completion of data input, a problem solution can be initiated. The program has modules for variable algorithm capabilities by using a macro instruction language which can be used to construct specific algorithms as needed.

Linear Problems

The user only needs to learn the mnemonics of the macro instruction language to use it. For example, the program instruction, TANG, is used to form the

Table A.2 Data Input: Macro Control Statements

Input Macro Control Cards—FORMAT (A4)

The input of each data segment is controlled by the value assigned to the control card, CC. The following values are admissible and each CC card must be immediately followed by the appropriate data (described in Tables A.3 to A.7).

CC Value	Data to be Input
COOR	Coordinate data
ELEM	Element data
MATE	Material data
BOUN	Boundary condition/joint-specification data
FORC	Prescribed nodal force/displacement data
PRIN	Print subsequent mesh data (default mode)
NOPR	Do not print subsequent mesh data
END	Must be last card in mesh data, terminates mesh input

Except for the END card the data segments can be in any order. If the values of FORC are zero, no input data is required.

Table A.3 Coordinate Data

Coordinate Data-FORMAT (2I5,7F10.0)
 (must immediately follow a COOR macro card)

The coordinate data card contains the node number N and the value of the coordinates for the node. The value of the spatial dimension input on the control card sets the number of coordinates required.

Nodal coordinates can be generated along a straight line described by the values input on two successive cards. The value of the node number is computed using the N and NG on the first card to compute the sequence $N, N+NG, N+2NG$, etc. Nodes need not be in order.

Columns	Description
1 to 5	Node number, N
6 to 10	Generator increment, NG
11 to 20	First coordinate
21 to 30	Second coordinate
31 to 40	Third coordinate

Terminate with blank card(s).

Table A.4 Element Data

Element Data-FORMAT (16I5)(must immediately follow an ELEM card)

The element data card contains the element number, material set number (which also selects the element type, see Table A.5), and the sequence of nodes connected to the element.

Elements must be in order with beam elements being numbered first. If element cards are omitted the element data will be generated from the previous element with the same material number and the nodes all incremented by the LX on the previous element. Generation to the maximum element number occurs when a blank card is encountered.

Columns	Description
1 to 5	Element number
6 to 10	Material set number
11 to 15	Node 1 number
16 to 20	Node 2 number
21 to 25	Generation increment, LX

Table A.5 Material Property Data

Material Data Sets

(must immediately follow a MATE macro card)

Each material property set also selects the element type which will be used for the material property data.

Card (1)-*FORMAT (I5,4X,I1,17A4)*

Columns	Description
1 to 5	Material set number (beam elements numbered first)
6 to 9	Not used
10	Element type number (beam element = 1, tendon element = 2, joint element = 3)
11 to 78	Alphanumeric information to be output

Each material Card (1) must be followed immediately by the material property data required for the element type being used.

Beam Element Data

Card (2)-*FORMAT (3I5)*

Columns	Description
1 to 5	Number of fibers
6 to 10	Number of stiffness Gaussian points (3)
11 to 15	Number of force Gaussian points (3)

Card (3)-FORMAT (4F10.0)

Columns	Description
1 to 10	Initial axial strain along the reference axis
11 to 20	Initial curvature at Gaussian point 1
21 to 30	Initial curvature at Gaussian point 2
31 to 40	Initial curvature at Gaussian point 3

Card(s) (4)-FORMAT (I5,2F10.0)

The element allows 4 types of materials to be coded as required in the beam element subroutine. This will read as many fibers as specified by Card (2).

Columns	Description
1 to 5	Material type of fiber (1 to 4)
6 to 15	Area of fiber
16 to 25	Distance of fiber centroid to reference axis

Tendon Element Data

Card (2)-FORMAT (6F10.0)

Columns	Description
1 to 10	First vertical eccentricity
11 to 20	First horizontal eccentricity
21 to 30	Second vertical eccentricity
31 to 40	Second horizontal eccentricity
41 to 50	Cross sectional area of tendon
51 to 60	Initial strain of tendon

Joint Element Data

Card (2)-FORMAT (F20.0, 2F10.0)

Columns	Description
1 to 20	Stiffness of joint element
21 to 30	Joint depth in the positive direction
31 to 40	Joint depth in the negative direction (magnitude)

Table A.6 Boundary Restraint/Joint Specification Data

Boundary Condition/Joint-Specification Cards-FORMAT (16I5)
(must immediately follow a BOUN macro card)

For each node which has at least one degree of freedom, DOF, with a specified displacement or is a final joint node, a card must be input. The convention used is:

- 1 no restraint, final joint node, force specified (located in columns 16 to 20);
- 0 no restraint, force specified; and
- 1 restrained, displacement specified,

where values of force or displacement input in FORC (Table A.7). Only joint specification can be generated.

Columns	Description
1 to 5	Node number
6 to 10	Generation increment
11 to 15	DOF 1 Code
16 to 20	DOF 2 Code
21 to 25	DOF 3 Code

Terminate with blank card(s).

Table A.7 Nodal Force Boundary Value Data

Force/Displacement Cards

(must immediately follow a FORC macro card)

Card(s) (1)-FORMAT (2I5, 7F10.0)

For each node which has a nonzero nodal force or displacement a force card must be input or generated. Generation is the same as for coordinate data (see Table A.3). The value specified is a force if the corresponding restraint code is -1 or 0, and a displacement if the code is 1. Forces specified at the final joint node override those specified at the initial joint node. Proportional numbers are specified at locations of incremental loads to be multiplied later by adequate loads.

Columns	Description
1 to 5	Node number
6 to 10	Generation increment
11 to 20	DOF 1 Force (Displacement)
21 to 30	DOF 2 Force (Displacement)
31 to 40	DOF 3 Force (Displacement)

Card (2)-Empty

Card(s) (3)-FORMAT (16I5)

Columns	Description
1 to 5	First node number with force to be incremented
6 to 10	Second node number with force to be incremented
	Etc.

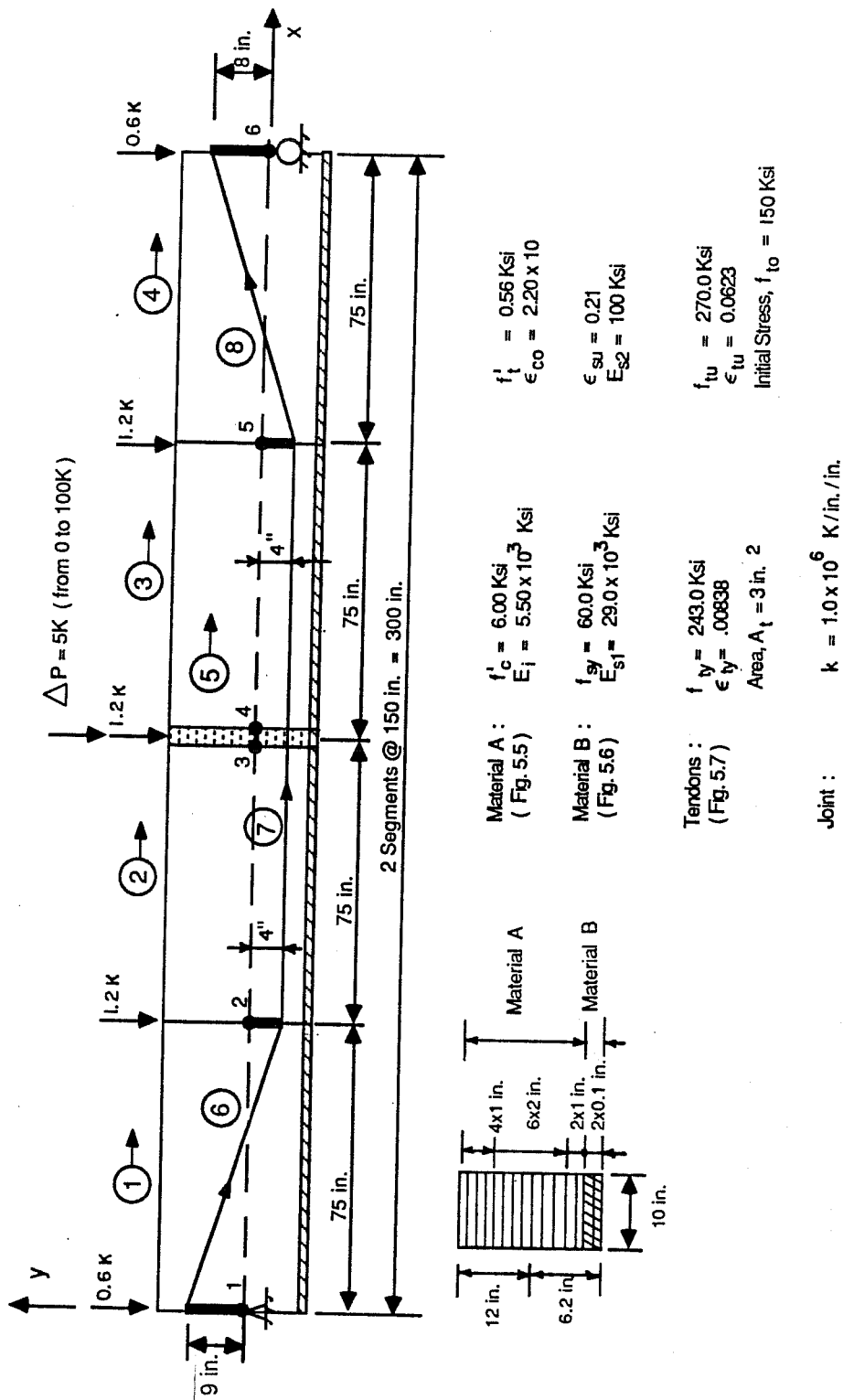


Fig. A.1 Mesh for externally prestressed segmental bridge with two segments.

Table A.8 Input Data for Externally Prestressed Segmental Bridge
of Fig. A.1

FEAP * EXTERNAL PRESTRESSED SIMPLE BEAM WITH 2 SEGMENTS **										
6	8	5	2	3	2	0	1	16	1	4
COOR										
1	1	0.								
3		150.								
4	1	150.								
6		300.								
ELEM										
1	1	1	2	1						
3	1	4	5	1						
5	2	3	4							
6	3	1	2							
7	4	2	5							
8	5	5	6							
BOUN										
1	0	1	1							
4			-1							
6			1							
MATE										
1	1									
14	3	3								
0.		0.		0.		0.				
1		10.		11.5						
1		10.		10.5						
1		10.		9.5						
1		10.		8.5						
1		20.		7.						
1		20.		5.						
1		20.		3.						
1		20.		1.						
1		20.		-1.						
1		20.		-3.						
1		10.		-4.5						
1		10.		-5.5						
2		1.		-6.05						
2		1.		-6.15						
2	3									
1000	000.			12.		6.2				
3	2									
9.		0.		-4.		0.		3.		.00517
4	2			-4.		0.		3.		.00517
-4.		0.		-4.		0.		3.		.00517
5	2			8.		0.		3.		.00517
-4.		0.								
FORC										
1				-0.6						
2				-1.2						
4				-1.0						
5				-1.2						
6				-0.6						
4										
END										

global symmetric stiffness matrix. If one wishes to form the right-hand side of the equations modified for specified displacements, one uses the program instruction, FORM. the resulting equations are solved using the instruction SOLV. Printed output can be obtained using the instructions DISP for the displacements and STRE for element variables such as strains, stresses, and internal forces. These instructions are sufficient to solve linear problems, that is, the macro instructions

TANG		FORM
FORM		TANG
SOLV	or:	SOLV
DISP		STRE
STRE		DISP

are the required instructions to solve any linear problem. The two modules produce the same algorithm except that element quantities and nodal displacements are printed in reverse order.

When multiple load problems are analyzed, the global stiffness matrix is always the same and need only be formed once. The right-hand side vector changes and the new displacements need to be computed. The procedure to solve more than one case at a time requires changing nodal loads and/or specified displacements. The macro instruction MESH causes the program to enter the data input module again, and at this stage loads can be changed. Data appears after the macro program instructions which terminate with the END statement for each case. To avoid repeating the same block of instructions for every loading case, looping commands are introduced as the instruction pair

```

      LOOP   n
      .
      .
      .
      .
      NEXT

```

which indicate that looping over all instructions between LOOP and NEXT will occur n times. Hence, the macro program for two load cases is

```

TANG
LOOP      2
MESH
FORM
SOLV
DISP
STRE
NEXT
END
FORC
                loads for problem 1
END
FORC
                loads for problem 2
END

```

The user should notice that the TANG instruction is executed only once while the SOLV instruction is executed twice.

A complete list of all available macro instructions are given in Table A.9. Many other classes of problems can be solved using these instructions.

Nonlinear Problems: Incremental-Load Method

The macro instruction program to solve a nonlinear problem by incrementing the load is given below. The program iterates at each step using the modified Newton-Raphson technique to achieve convergence. Summarized descriptions are given for some instructions.

TABLE A.9 LIST OF MACRO PROGRAMMING COMMANDS

The following is a list of macro instruction commands which can be used to construct solution algorithms. The first instruction must be a card with MACR in columns 1 to 4.

Columns 1 to 4	Columns 11 to 15	Description
CONV		Displacement convergence test
DISP	N	Print nodal displacements every N steps in loop
DT	V	Set time increment to value V
FORM		Form right hand side of equations and tests internal force convergence
LOOP	N	Loop N times over all instructions between LOOP and matching NEXT instruction
MESH		Input mesh changes (must not change boundary conditions). Data follows macro program
NEXT		End of loop instruction
PROP	1	Input proportional load table (data follows macro program)
SOLV		Solve tangent equations. Updates nodal displacement
STRE	N	Print element variables (strains, stresses, internal forces, joint width, etc.) every N steps in loop
TANG		Symmetric tangent stiffness formulation
TIME		Advance time by ΔT value
TOL	V	Set solution convergence tolerance to value V (default value = 1.0×10^{-9})
END		End of macro program instructions. Data for program follows in order of use

```

DT      .1    Δt = .1
PROP    1     calculates PROP to be multiplied by
           input loads to be incremented
LOOP    10    increment loop
TIME    t = t + Δt
LOOP    3     modified Newton-Raphson iteration loop
TANG    compute  $\underline{K}_t$ 
LOOP    5     tangent stiffness is reformed every 5
           iterations
FORM    compute right-hand side vector
SOLV    compute  $\underline{U}$  and  $\underline{U} = \underline{U} + \Delta \underline{U}$ 
CONV    check displacement convergence
NEXT
DISP    print  $\underline{U}$ 
NEXT
STRE    print stresses and internal forces
NEXT
END

```

A proportional loading is permitted with

$$\text{PROP} = A1 + A2 \times t + A3 \times (\sin(A4 \times t + A5))^L$$

where the coefficients are input on a data card following the END macro card according to Table A.10. The midspan load in Fig. A.1 requires $\text{PROP} = 1.2 + 5.0 \times t$ where $\Delta t = 1.0$ and t increases from 0.0 to 20.0.

TABLE A.10 PROPORTIONAL LOAD DATA

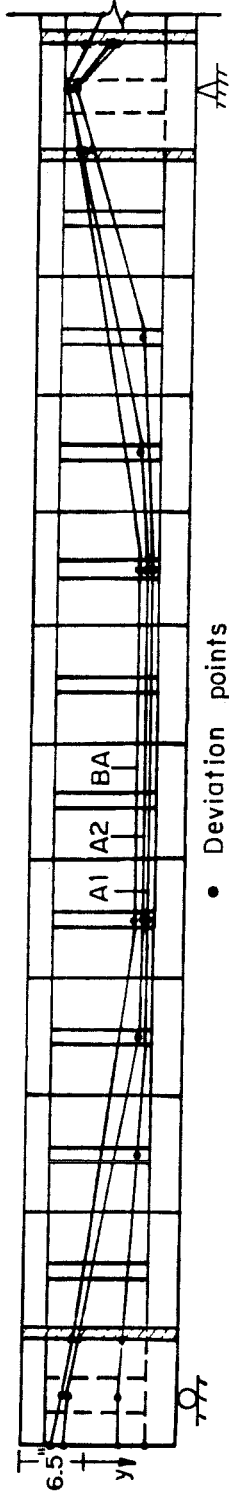
PROPORTIONAL LOAD CARD-FORMAT (2I5,7F10.0)

Columns	Description
6 to 10	L
11 to 20	t (min.), minimum time for which PROP is computed
21 to 30	t (max.), maximum time for which PROP is computed
31 to 40	A1
41 to 50	A2
51 to 60	A3
61 to 70	A4
71 to 80	A5

APPENDIX B
GEOMETRY AND STRESSES FOR EXTERNAL
TENDONS IN CHAPTER 5

Figure B.1 provides some of the properties of the prestressing tendons for the model bridge considered in Chapter 5. The reference axis is located at 6.5 in. from the top, and a positive vertical direction is selected downward. Y gives the vertical coordinate of the anchorages or deviation points of the tendons located above the values of Y . The transfer forces between consecutive points are given by P_t , while P_∞ gives the tendon forces after losses.

Span A:



• Deviation points

TENDON # A1: $10 - \frac{3}{8}$ " ϕ , $A_{ps} = 0.85 \text{ in.}^2$

(in.)	y	3.5	3.99	5.75	6.33	6.33	5.75	-0.77	-2.57	134
P	161	161	161	157	153	149	144	138	134	
P	145	145	140	136	133	127	123	119		

TENDON # A2: $10 - \frac{3}{8}$ " ϕ , $A_{ps} = 0.85 \text{ in.}^2$

(in.)	y	-2.0	-0.87	5.75	6.04	6.04	5.75	-1.48	-2.71	126
P	161	160	159	154	150	146	141	134	126	
P	145	144	143	139	135	132	127	120	113	

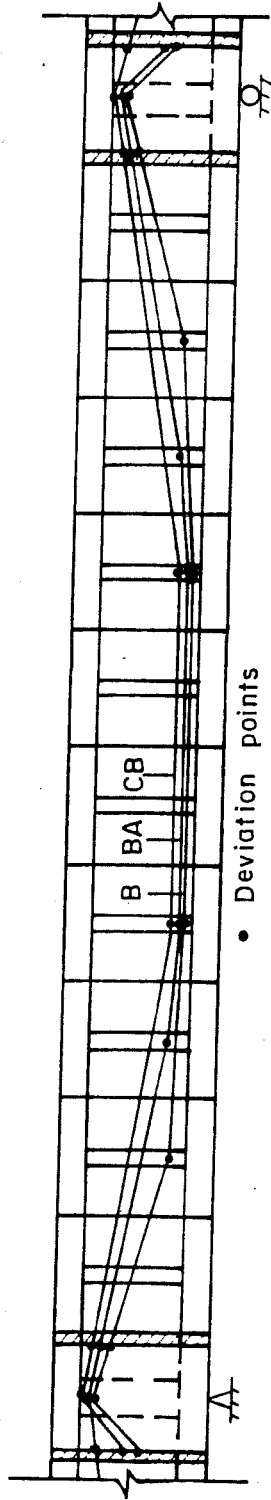
TENDON # BA: $4 - \frac{3}{8}$ " ϕ , $A_{ps} = 0.34 \text{ in.}^2$

(in.)	y	-2.0	-1.15	5.75	5.75	5.75	-1.84	-2.78	127	
P	64.4	64.0	63.6	62.5	61.3	59.6	58.7	57.9	57.5	
P	57.9	57.5	57.1	56.2	55.1	53.6	52.8	52.0	51.5	

Fig. B.1 Geometry and prestressing forces at transfer and after losses for each tendon

to be continued

Span B:



• Deviation points

TENDON # B : $10 - \frac{3}{8}$ " ϕ , $A_{ps} = 0.85 \text{ in.}^2$

Y	2.64	-0.82	5.75	6.33	6.33	5.75	-0.82	2.64
P	112	119	126	131	134	138	144	153
P	101	105	109	115	118	122	127	136
								145

TENDON # BA : $4 - \frac{3}{8}$ " ϕ , $A_{ps} = 0.34 \text{ in.}^2$

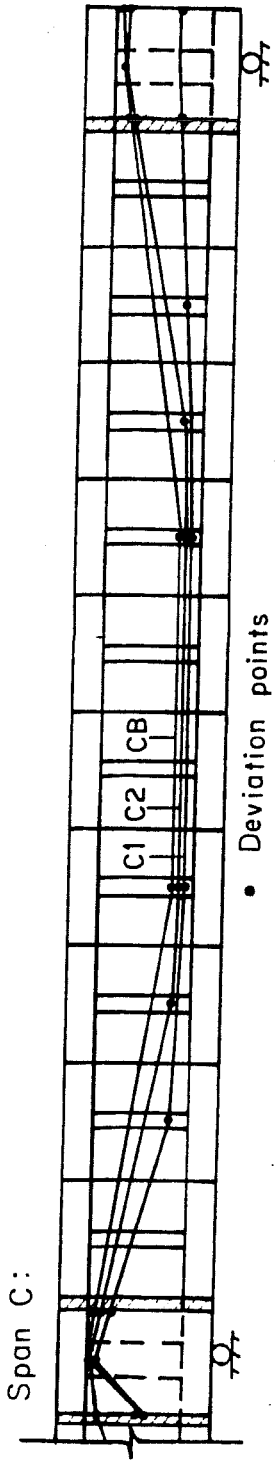
Y	2.76	-1.54	5.75	6.04	6.04	5.75	-1.54	2.76
P	60	59.6	58.7	56.3	54.8	53.5	51.2	48.7
P	54.3	53.6	52.8	50.6	49.3	48.1	46.0	43.8
								41.5

TENDON # CB : $4 - \frac{3}{8}$ " ϕ , $A_{ps} = 0.34 \text{ in.}^2$

Y	2.85	-1.91	5.75	5.75	5.75	5.75	-1.91	2.85
P	51.5	53.9	56.3	57.4	57.4	58.7	59.5	60.4
P	46.3	49.0	50.6	51.6	51.6	52.7	53.5	54.2
								59

Fig. B.1 Continued

to be continued



TENDON # C1: $10 - \frac{3}{8}$ " ϕ , $A_{ps} = 0.85 \text{ in.}^2$

γ	2.57	-0.77	5.75	6.33	6.33	5.75	3.99	3.5	1.9
P_t	134	138	144	149	153	157	161	161	161
P_{e0}	119	123	127	133	136	140	145	145	145

TENDON # C2: $10 - \frac{3}{8}$ " ϕ , $A_{ps} = 0.85 \text{ in.}^2$

γ	2.71	-1.48	5.75	6.04	6.04	5.75	6.04	5.75	2.0
P_t	126	134	141	146	150	154	159	160	161
P_{e0}	113	120	127	132	135	139	143	144	145

TENDON # CB: $4 - \frac{3}{8}$ " ϕ , $A_{ps} = 0.34 \text{ in.}^2$

γ	2.85	-1.91	61.2	5.75	5.75	63.6	-1.15	-2.0	1.0
P_t	59.5	60.4	61.2	62.5	62.5	63.6	64.0	64.4	64.4
P_{e0}	53.5	54.2	55.0	56.2	56.2	57.1	57.5	57.9	57.9

Fig. B.1 Continued

REFERENCES

1. ACI Committee 318, *Building Code Requirement for Reinforced Concrete* (ACI 318-83), November, 1983.
2. Bathe, K.J., *Finite Element Procedures in Engineering Analysis*, Prentice-Hall, Englewood Cliffs, N.J., 1982.
3. Mondkar, D.P., and Powell, G.H., "Evaluation of solution schemes for nonlinear structures," *Computer and Structures*, Vol. 9, September, 1977, pp. 223-236.
4. Sabouri, A.R., and Gergeley, P., "Finite Element Analysis of R/C Frames and Framewall Systems," *Proceedings, Ninth Conference on Electronic Conference*, ASCE, K.M. Will, ed., 1986, pp. 579-589.
5. Weaver Jr., W., and Johnston, P.R., *Finite Elements for Structural Analysis*, Prentice-Hall, Englewood Cliffs, N.J., 1984.
6. Zienkiewicz, O.C., *The Finite Element Method*, 3rd. ed., McGraw-Hill, Ltd., London, 1977.

VITA

Kamal Chakib El-Habr was born in Mansourieh Bhamdoun in Lebanon, on August 14, 1961, the son of Chakib Amin El-Habr and Mariam Georges El-Habr. He attended Saint Joseph Elementary School, Shanay Intermediate School, and Ashrafyey and Bhamdoun Secondary Schools. After successfully completing the Lebanese General Official Exam in 1978, he supervised the family farm for two years. He attended Beirut University College in Beirut, Lebanon, between the summers of 1980 and 1982. He transferred to The University of Texas at Austin in Austin, Texas, and received the degree of Bachelor of Science in Civil Engineering, with highest honors, in August 1984. He then entered the Graduate School of the University of Texas at Austin. During that period, he worked as a tutor for the College of Engineering and as a teaching assistant and research assistant. He also worked in the renovation of houses, and started a private tutoring service.

Permanent Address: Mansourieh Bhamdoun
ALEY, LEBANON

This thesis was typed by Kamal C. El-Habr.